Ultrasonics Sonochemistry 135 (2026) 108152

Contents lists available at ScienceDirect

Ultrasonics Sonochemistry

journal homepage: www.elsevier.com/locate/ultson

Stage-dependent thermo-ultrasonic intervention modulates structural evolution and paste properties of corn starch during the gelatinization transition

Houhua Wang [a,b], Yuanyuan Li [c], Tianpeng Chen [d], Wenjun Wang [a,b], Donghong Liu [a,b], Shuang Qiu [a,b,d,*]

[a] College of Biosystems Engineering and Food Science, Zhejiang University, Hangzhou 310058, China
[b] Future Food Laboratory, Innovative Center of Yangtze River Delta, Zhejiang University, No. 828, Zhongxing Road, Xitang Town, Jiashan County, Jiaxing, Zhejiang Province 314102, China
[c] The State Key Laboratory of Subtropical Silviculture, Bamboo Industry Institute, Zhejiang Agriculture & Forestry University, Hangzhou 311300, Zhejiang, China
[d] Mantang Qingyang (Jiaxing) Health Technology Co., Ltd., Jiaxing, Zhejiang Province 314102, China

ARTICLE INFO

Keywords:
Corn starch
Ultrasound treatment
Gelatinization stage
Rheological properties
Molecular organization
Two-dimensional correlation spectroscopy

ABSTRACT

Although the effects of ultrasound on native and fully gelatinized starch have been widely investigated, its effects during the gelatinization transition remain largely unexplored. This study evaluated the physicochemical and structural modifications in corn starch subjected to ultrasonic treatment at 60, 69, and 73 °C. These temperatures corresponded to the pre-gelatinization, gelatinization-onset, and gelatinization-peak temperatures, respectively. Ultrasound applied at 60 °C promoted starch swelling without compromising the viscoelastic properties of the fully gelatinized paste. Structural characterization indicated that samples sonicated at 60 °C retained characteristic crystalline diffraction features and relatively preserved short-range molecular organization. In contrast, ultrasound applied at 69 and 73 °C significantly reduced paste consistency and viscoelastic strength, accompanied by extensive disruption of granular morphology and molecular organization. Iodine-binding analysis confirmed that ultrasound altered the amount and iodine-complexing capacity of soluble starch fractions in a stage-dependent manner. Overall, this study demonstrates that the structural state of starch at different stages of the gelatinization transition governs its response to ultrasonic modification. This work provides a mechanistic basis for modulating starch hydration and rheological properties via precisely timed ultrasound intervention during thermal processing.

1. Introduction

As an abundant and renewable polysaccharide, starch is widely used as a nutritional component and a structural matrix in the food and materials industries. Despite its versatility, native starch often fails to meet rigorous industrial processing demands owing to its poor cold-water solubility, tendency toward retrogradation, and sensitivity to thermal and mechanical stresses. To overcome these application barriers in complex systems [1], physical modification strategies have emerged as promising and eco-friendly alternatives to tailor starch functionality without relying on chemical modification.

Starch gelatinization is a progressive structural transition rather than an instantaneous event. When heated in sufficient water, starch granules undergo gradual hydration and swelling, followed by disruption of intermolecular interactions, progressive loss of detectable crystalline order, increased molecular mobility, release of soluble starch components, and eventual formation of a continuous or particulate paste network [2]. At the supramolecular level, this transition involves hydration of amorphous regions and progressive disruption of ordered nanocrystalline domains, accompanied by changes in local molecular organization [3]. These structural changes occur concurrently with granule swelling, crystalline order disruption, and the development of a continuous paste network [3,4]. Consequently, the structural integrity, water accessibility, and molecular mobility of the starch matrix vary

* Corresponding author at: No. 828, Zhongxing Road, Xitang Town, Jiashan County, Jiaxing, Zhejiang Province 314102, China.
E-mail addresses: houhua_wang@foxmail.com (H. Wang), yuanli@zafu.edu.cn (Y. Li), 18611863043@163.com (T. Chen), wangwj@zju.edu.cn (W. Wang), sq16@zju.edu.cn (S. Qiu).

https://doi.org/10.1016/j.ultsonch.2026.108152
Received 24 July 2026; Received in revised form 4 November 2026; Accepted 8 November 2026
Available online 10 November 2026
1350-4177/© 2026 The Author(s). Published by Elsevier B.V. This is an open access article under the CC BY license (http://creativecommons.org/licenses/by/4.0/).

substantially across the pre-gelatinization, onset, peak, and post-gelatinization stages [5]. Evidence from other polysaccharide systems indicates that the timing and intensity of physical-field intervention can fundamentally influence the physicochemical properties of the final polymer network [6–8]. For example, in TEMPO-oxidized cellulose nanocrystal suspensions, 30–120 s of sonication transformed heterogeneous fiber aggregates into a weak physical gel, with the 120 s treatment yielding a highly homogeneous, transparent gel exhibiting 97 % transmittance at 500 nm [7]. During the cold-set gelation of κ-carrageenan, ultrasound treatment at 50–150 W enhanced the textural properties of the gel up to an optimal duration of ~ 2.5 min; however, prolonged sonication beyond this threshold induced structural degradation, weakening the gel and reducing intrinsic viscosity [8]. These findings demonstrate that physical treatment conducted during polysaccharide phase transitions can either promote or disrupt network formation, depending on the application timing and the structural state of the biopolymer. Recent crystallographic studies have further revealed that starch granules contain intrinsic nanocrystalline domains, which contribute to the characteristic X-ray diffraction patterns and represent important components of starch hierarchical organization [3,4,9].

Ultrasound-induced cavitation may influence starch at multiple hierarchical structural levels, including granular morphology, semicrystalline organization containing ordered nanocrystalline domains, and molecular interactions, depending on the physical state of the starch matrix [10]. At the granular level, structural changes involve hydration, swelling, and disruption of granule integrity. At the semicrystalline level, starch contains nanocrystalline domains embedded within a less ordered matrix. These domains exhibit orthorhombic and/or hexagonal crystal structures and contribute to the characteristic X-ray diffraction patterns of starch. At the molecular level, structural changes are discussed in terms of hydrogen bonding, chain mobility, and local molecular organization, separately from the crystallographic description of the nanocrystalline domains [11]. When applied to native starch granules, acoustic energy primarily induces surface erosion, localized defects, and increased water accessibility, while the overall granular morphology is generally preserved before gelatinization. For example, ultrasound treatment at 20 kHz and 170 W for 30 min increased the porosity of rice, corn, wheat, and potato starch granules without a complete loss of granular morphology [12]. Ultrasound-treated pea starch showed surface pits and micropores, accompanied by a decrease in relative crystallinity from 26.3 % to 24.9 % and a reduction in peak viscosity from 3990 to 3582 cP [13]. Under thermo-ultrasonic conditions, the extent of granule damage is highly dependent on treatment temperature and duration. Corn starch sonicated at 65 °C for 30 min mainly exhibited granule swelling, while a 60-min exposure caused more severe disruption and the formation of an amorphous matrix [14]. In contrast, in post-gelatinization systems, swollen starch structures and hydrated starch molecules are directly exposed to acoustic energy. Iida et al. reported that post-gelatinization sonication could liquefy 20–30 % starch gels and reduce the viscosity of 5–10 % starch solutions by approximately two orders of magnitude within 30 min [15]. These findings indicate that the structural susceptibility of starch to ultrasound is strictly dependent on its gelatinization state. However, ultrasound intervention during the active transition region of the gelatinization process remains poorly understood [16].

In this study, ultrasound was applied to corn starch suspensions at 60, 69, and 73 °C, corresponding to pre-gelatinization, gelatinization-onset, and gelatinization-peak conditions, respectively, as determined by differential scanning calorimetry (DSC). Samples collected immediately after intervention (NCG) and samples subsequently heated to 95 °C (CG) were systematically evaluated. We hypothesized that ultrasound applied prior to the main gelatinization transition would mainly promote starch hydration and swelling while preserving the granular framework. Acoustic intervention within the onset-to-peak temperature range would disrupt the hydrated granules, resulting in a compromised final paste network. This study investigates how thermo-ultrasonic intervention at different stages of the starch gelatinization transition influences structural characteristics and paste properties, providing insights into the stage-dependent regulation of starch functionality during thermal processing.

2. Materials and methods

2.1. Materials and reagents

Corn starch (botanical source: *Zea mays* L.) was supplied by Jingshan Siyun Trading Co., Ltd. (Hubei, China). According to the manufacturer, the starch powder had an apparent amylose content of approximately 27.5 % and contained 11.2 % moisture, 0.35 % crude protein, 0.15 % crude lipid, and 0.08 % ash. Fluorescein 5(6)-isothiocyanate (FITC), trichloroacetic acid (TCA), potassium iodide (KI), iodine (I_2), potassium bromide (KBr), dimethyl sulfoxide (DMSO), lithium bromide (LiBr), pullulan standards, and potato amylose (PA) were of analytical grade and purchased from Aladdin Biochemical Technology Co., Ltd. (Shanghai, China). Deionized water was used throughout all experiments.

2.2. Preliminary DSC analysis and selection of intervention temperatures

The gelatinization state was evaluated based on DSC thermal transitions, including the presence or absence of endothermic peaks and changes in gelatinization enthalpy (ΔH), rather than solely based on the intervention temperature. Preliminary differential scanning calorimetry (DSC) analysis of native corn starch was performed using a DSC 300 Caliris instrument (NETZSCH, Germany) to determine the gelatinization temperature range and select the ultrasound intervention temperatures. Native starch powder (~3 mg) was weighed into an aluminum pan, and deionized water was added at a starch-to-water mass ratio of 1:3 (w/w). The pans were hermetically sealed and equilibrated at ambient temperature for 24 h. Thermal scanning was conducted from 20 to 100 °C at a heating rate of 5 °C/min under a nitrogen flow of 20 mL/min, using an empty sealed aluminum pan as the reference.

2.3. Starch thermo-ultrasonic treatment

Corn starch suspensions (5 %, w/v) were prepared by dispersing starch powder in deionized water under continuous magnetic stirring. For each treatment, 150 mL of starch suspension was placed in a 250 mL glass beaker. Before heating to the intervention temperature, all suspensions were first equilibrated at 50 °C so that they entered the subsequent heating step from the same starting temperature.

For ultrasound treatment, starch suspensions were sonicated at 60, 69, 73, or 95 °C, respectively, using a probe-type ultrasonic processor (JY92-IIDN, Scientz Biotechnology Co., Ltd., Ningbo, China) equipped with a 6 mm diameter titanium probe. The probe tip was positioned 2 cm above the bottom of the beaker. Ultrasound was applied at a frequency of 20 kHz with a nominal power setting of 270 W in a pulsed mode (1 s on and 1 s off) for 5 min. Based on the nominal power setting (270 W) and the treatment volume (150 mL), the corresponding nominal power density and nominal energy input density were calculated as 1.8 W/mL and 270 J/mL, respectively, considering the 50 % duty cycle. During sonication, the treatment vessel was placed in a thermostatically controlled circulating water bath to maintain the treatment temperature, and the sample temperature was recorded using an electronic thermometer. The corresponding controls were prepared using the same suspension volume and subjected to the same heating program and treatment duration, with the ultrasound generator switched off. Specifically, after equilibration at 50 °C, samples were heated to the designated intervention temperatures (60, 69, and 73 °C) and maintained for the same duration as the ultrasonic groups. The NU samples were then subjected to the same subsequent heating process to 95 °C for CG preparation, without ultrasonic irradiation. Therefore, the U and NU

samples experienced identical thermal histories, and the differences between them were attributed to the ultrasonic treatment.

Starch suspensions were separately prepared for two experimental groups: an incompletely gelatinized (NCG) group and a completely gelatinized (CG) group. For the NCG group, heating was terminated immediately after acoustic treatment at 60, 69, and 73 °C, respectively, and the 60-U-NCG, 69-U-NCG and 73-U-NCG samples were collected for subsequent analyses. For the CG group, 60-U-CG, 69-U-CG, 73-U-CG starch suspensions were ultrasonically treated at the designated intervention temperatures and subsequently heated to 95 °C. The total thermal processing time was maintained at 25 min for all CG samples. In addition, 95-U-CG and 95-NU-CG samples were prepared as a fully gelatinized reference group by heating the suspensions directly to 95 °C, with or without ultrasound treatment at 95 °C, respectively. Freshly prepared samples were used for rheological measurements, particle-size analysis, swelling-power determination, iodine-binding analysis, and CLSM observation. Separate portions intended for structural characterization were immediately frozen using liquid nitrogen, stored at − 80 °C for 24 h, and freeze-dried for 48 h. The freeze-dried powders were stored in a desiccator until further use. In this study, NCG and CG were defined according to the sample preparation procedure rather than as absolute gelatinization categories. NCG samples were collected immediately after ultrasound treatment at the selected intervention temperatures without subsequent heating to 95 °C. CG samples were obtained after further heating to 95 °C to evaluate the final paste properties after thermal processing. Therefore, the designation of NCG indicates the sampling stage after ultrasound intervention and does not necessarily represent a fixed incomplete gelatinization state.

The experimental design comprised 14 treatment groups: four independently prepared groups at each intervention temperature (60, 69, and 73 °C), and two completely gelatinized groups at 95 °C. The sample codes and corresponding treatment conditions are summarized in Table 1.

2.4. Rheological measurements

The rheological properties of the starch pastes were evaluated using a rotational rheometer (MCR302, Anton Paar, Graz, Austria) equipped with a parallel-plate geometry (20 mm diameter, 1000 μm gap size). Following gelatinization, the samples were transferred onto the rheometer plate, and the exposed edges were coated with a thin layer of silicone oil to prevent moisture evaporation. Prior to measurement, all samples were equilibrated at 25 °C for 20 min to allow for thermal equilibration and structural relaxation.

2.4.1. Steady-state shear and thixotropy

Steady shear measurements were performed at 25 °C to evaluate the flow behavior and thixotropy of the samples. The shear rate was programmed as a continuous ramp, increasing linearly from 5 to 131 s^{-1} (upward curve) and subsequently decreasing back to 5 s^{-1} (downward curve). To mathematically describe the flow characteristics, the shear stress data from both the upward and downward sweeps were fitted to the Herschel-Bulkley model (Equation (1) [17]:

$$\tau = \sigma^0 + K\gamma^n \tag{1}$$

where τ represents the shear stress (Pa), σ_0 is the yield stress (Pa), K denotes the consistency index (Pa·s^n), γ is the shear rate (s^{-1}), and n is the flow behavior index. Furthermore, the extent of thixotropy was quantitatively evaluated by calculating the hysteresis loop area integrated between the upward and downward shear curves.

Table 1
Sample information and treatment conditions.

Temperature (°C)	Group with ultrasound treatment (U)		Group without ultrasound treatment (NU)	
	NCG	CG	NCG	CG
60	60-U-NCG	60-U-CG	60-NU-NCG	60-NU-CG
69	69-U-NCG	69-U-CG	69-NU-NCG	69-NU-CG
73	73-U-NCG	73-U-CG	73-NU-NCG	73-NU-CG
95	—	95-U-CG	—	95-NU-CG

U, ultrasound-treated; NU, non-ultrasound-treated; NCG, samples collected immediately after treatment at the designated intervention temperature; CG, samples were subjected to ultrasound treatment at the designated intervention temperatures and subsequently heated to 95 °C. NCG and CG samples were prepared from separate starch suspensions and were treated as independent experimental groups.

2.4.2. Dynamic oscillatory shear

Dynamic oscillatory measurements were conducted to evaluate the viscoelastic properties of the samples. An initial strain sweep test (0.01 %–100 % strain at 1 Hz) was performed to determine the linear viscoelastic region (LVR) of the starch gels. Subsequently, the oscillatory shear tests were conducted over an angular frequency range of 0.1 to 100 rad/s at 25 °C. Frequency sweep measurements were performed at a constant strain amplitude of 1 %, which was within the linear viscoelastic region of all samples, over the angular frequency range investigated. The storage modulus (G') and loss modulus (G'') were recorded as functions of the angular frequency.

2.5. Starch hydration extent and iodine-binding properties

2.5.1. Particle size distribution of hydrated starch

The particle size distribution (PSD) of the starch pastes was characterized using a laser diffraction particle size analyzer (Mastersizer 3000, Malvern Instruments Ltd., Worcestershire, UK). Prior to analysis, the samples were equilibrated to 25 °C for 24 h. To prevent multiple scattering effects, the pastes were gradually introduced into the dispersion unit containing deionized water until an obscuration level of 6 %–10 % was achieved. Continuous agitation was maintained throughout the measurement to ensure a homogeneous dispersion and prevent particle sedimentation. The refractive indices were set at 1.53 for the starch particles and 1.33 for the dispersant (water).

2.5.2. Swelling power and iodine-reactive amylose-equivalent content

The swelling power and leached amylose content were determined via a centrifugation method. The starch pastes were equilibrated at 25 °C for 60 min, followed by centrifugation at 12,000 × g for 20 min. The supernatant was decanted and reserved for leached amylose analysis, and the wet sediment was weighed (W_{wet}). Subsequently, the sediment was dried in an oven at 105 °C to a constant mass (W_{dry}). The swelling power (SP) was calculated using Equation (2):

$$SP\left(\frac{g}{g}\right) = \frac{W_{wet}}{W_{dry}} \tag{2}$$

Swelling power was calculated as the ratio between the weight of the hydrated starch sediment after centrifugation and the initial dry starch weight. This value represents the amount of water retained by starch structures per unit mass of dry starch and reflects the hydration capacity and swelling ability of starch.

The leached amylose concentration in the supernatant was quantified using the iodine colorimetric assay. An aliquot (3 mL) of the supernatant was mixed with 4 mL of NaOH (0.33 M) and incubated in a boiling water bath for 30 min. Upon cooling to ambient temperature, 4 mL of TCA (5 %, w/v) was introduced to adjust the pH to approximately 5.5, followed by the addition of 1 mL of iodine-potassium iodide solution (0.01 M I_2 / 0.1 M KI). The mixture was incubated in the dark for 30 min. The solution was then diluted 20-fold with deionized water, and the absorbance was recorded at 620 nm using a UV–vis spectrophotometer. The amylose concentration was determined against a standard curve generated with pure potato amylose, with the absorbance values of all test samples strictly falling within the linear range. Deionized water was

subjected to identical reagent treatments and served as the blank control.

2.5.3. Iodine-binding absorption spectra of soluble starch

The UV–visible absorption spectra of starch–iodine complexes were recorded to compare the iodine-binding characteristics of soluble starch. The supernatants obtained after centrifugation, as described in Section 2.5.2, were used for spectral analysis. The supernatants were diluted 1000-fold with deionized water before analysis. An aliquot (20 mL) of each diluted supernatant was mixed with 400 μL of iodine–potassium iodide solution (0.01 M I_2/0.1 M KI). The mixture was incubated in the dark at room temperature for 30 min before measurement. A blank was prepared by replacing the starch supernatant with an equal volume of deionized water and subjecting it to the same reagent treatment. An untreated native corn starch suspension was prepared at the same starch concentration as the experimental samples, receiving neither thermal nor ultrasound treatment. The absorption spectra were recorded from 400 to 900 nm using a UV–visible spectrophotometer. The maximum absorption wavelength (λ_{max}) and the absorbance at 620 nm (OD620) were obtained to compare the spectral position and iodine-binding capacity of the soluble starch.

2.5.4. DSC analysis of treated samples

To evaluate the remaining gelatinization transition after treatment, the freeze-dried starch samples were analyzed using the same starch-to-water ratio, equilibration procedure, and thermal-scanning program described in Section 2.2. The onset temperature (T_o), peak temperature (T_p), conclusion temperature (T_c), and gelatinization enthalpy (ΔH) were determined from the thermograms. Enthalpy values were expressed as J/g of dry starch.

2.6. Morphological characterization

2.6.1. Scanning electron microscopy

The surface morphology of the freeze-dried starch powders was characterized using a scanning electron microscope (Gemini SEM 360 SEM; ZEISS; Germany). Prior to observation, the samples were affixed to aluminum stubs via double-sided conductive carbon tape and sputter-coated with a thin layer of gold to enhance conductivity and minimize electron charging artifacts. Representative micrographs were acquired at an accelerating voltage of 3.0 kV and a magnification of 1000 × .

2.6.2. Confocal laser scanning microscope

The microstructural characteristics of the starch pastes were examined using a confocal laser scanning microscope (CLSM, LSM 900, Carl Zeiss Microscopy GmbH, Jena, Germany). A stock solution of FITC (2 mg/mL) was prepared in deionized water. For fluorescent staining, 20 μL of the FITC solution was homogeneously mixed with 1 mL of the starch paste. An aliquot of the stained sample was transferred to a concave glass slide and sealed with a coverslip without physical compression. To minimize fluorescence quenching and moisture evaporation, image acquisition was completed within 15 min of preparation. Excitation was performed at 488 nm, and the corresponding emission signals were collected in the range of 500–525 nm. CLSM images were obtained utilizing a 20 × objective lens.

2.7. Structural characterization

2.7.1. X-ray diffraction analysis

X-ray diffraction (XRD) patterns of the starch samples were acquired using an X-ray diffractometer (Rigaku SmartLab SE, Rigaku, Tokyo, Japan). Prior to analysis, the lyophilized starch powders were compacted into the sample holder to yield a uniform analytical surface. Measurements were performed using Cu-Kα radiation (λ = 0.154 nm) operating at 40 kV and 40 mA. The diffractograms were recorded over a 2θ range of 5° to 40° with a step size of 0.02° and a scanning speed of 2°/min [18]. Second-derivative analysis of the XRD profiles was performed to assist in identifying diffraction peak positions. The identified reflections were indexed by comparison with the crystallographic data reported by Rodriguez-Garcia et al [11].

2.7.2. Fourier-transform infrared (FTIR) spectroscopy

FTIR spectra of the starch samples were recorded using a Nicolet iS50 FTIR spectrometer (Thermo Fisher Scientific, USA). Lyophilized starch powder (1 mg) was thoroughly mixed with 100 mg of spectroscopic-grade anhydrous KBr and compressed to a translucent pellet. A pure KBr pellet was used to collect the background spectrum. Spectra were recorded over the range of 4000–400 cm^{-1} at a resolution of 4 cm^{-1}, with 32 scans accumulated for each spectrum. All spectra were subjected to the same baseline-correction and normalization procedures before comparison.

2.7.3. Two-dimensional correlation spectroscopy

Generalized two-dimensional correlation spectroscopy (2D-COS) was employed to compare temperature-dependent spectral variations among starch samples treated at different ultrasound intervention temperatures [19,20]. The intervention temperatures of 60, 69, and 73 °C were used as the external perturbation variables. Four independent spectral series were constructed and analyzed separately:

- NU-NCG: 60-NU-NCG, 69-NU-NCG, and 73-NU-NCG;
- U-NCG: 60-U-NCG, 69-U-NCG, and 73-U-NCG;
- NU-CG: 60-NU-CG, 69-NU-CG, and 73-NU-CG;
- U-CG: 60-U-CG, 69-U-CG, and 73-U-CG.

Native starch and samples treated at 95 °C were excluded from 2D-COS analysis as native starch received neither ultrasound nor thermal treatment, and the 95 °C group (95-NU-CG, 95-U-CG) served as a fully gelatinized reference. Before 2D-COS analysis, all FTIR spectra were subjected to baseline correction and normalization. Synchronous, $\Phi(\nu_1,\nu_2)$, and asynchronous, $\Psi(\nu_1,\nu_2)$, correlation maps were calculated using 2Dshige software (Kwansei-Gakuin University, Japan). The synchronous maps were used to identify spectral bands that changed with increasing intervention temperatures, and the asynchronous maps were used to resolve spectral variations that were not fully synchronized. Where clearly resolved cross-bands were present in both maps, the relative sequence of spectral changes was evaluated according to Noda's rules. At a given coordinate, identical signs of the synchronous and asynchronous Cross-bands indicate that the spectral change at ν_1 precedes that at ν_2 along the increasing-temperature series, whereas opposite signs indicate the reverse sequence [21]. The analysis focused on the O–H stretching region at 3680–3000 cm^{-1}, the water-associated region at 1750–1550 cm^{-1}, and the starch fingerprint region at 1200–900 cm^{-1}. Because each treatment group contained only three intervention temperatures, the asynchronous maps and the derived sequence of spectral changes were interpreted as exploratory indicators of temperature-dependent band variation.

2.7.4. Apparent molecular-weight analysis

The molecular weight distributions of the treated starch samples were evaluated using a gel permeation chromatography (GPC) system consisting of an Agilent PL-GPC220 (Agilent 1100 HPLC, Agilent, America) instrument equipped with a Waters 1525 pump. The freeze-dried samples were dispersed in HPLC-grade dimethyl sulfoxide (DMSO) containing 50 mM LiBr at a concentration of 2 mg/mL. To disrupt intermolecular hydrogen bonds and ensure dissolution, the mixtures were agitated at 80 °C for 2 h. Prior to injection, all solutions were passed through a 0.45 μm PTFE syringe filter. The DMSO/LiBr solution served as the mobile phase, delivered at a constant flow rate of 0.6 mL/min. Chromatographic separation was performed on an Agilent PLgel 5 μm MIXED-C column (300 × 7.5 mm) maintained at 80 °C to minimize solvent viscosity increase and prevent polymer re-aggregation.

The system was calibrated using narrowly distributed pullulan standards. The number-average (M_n), weight-average (M_w), Z-average (M_z), peak molecular weight (M_p), the polydispersity index (PDI = M_w/M_n), and the distribution width coefficient (M_z/M_w), were determined using ASTRA 6.1 software (Wyatt Technology, CA, USA).

2.7.5. Solid-state ^{13}C CP/MAS NMR spectroscopy

Solid-state ^{13}C cross-polarization magic-angle spinning (CP/MAS) NMR spectra were acquired using an NMR spectrometer (Bruker Avance Neo 400WB, Bruker, Germany) operating at a ^{13}C resonance frequency of 100.6 MHz. The starch samples were compacted into 4 mm ZrO_2 rotors. The measurements were conducted at a magic-angle spinning rate of 8 kHz, utilizing a contact time of 1.5 ms and a recycle delay of 2 s. A total of 2048 scans were accumulated per sample. Chemical shifts were externally calibrated against the methylene signal of adamantane at 29.5 ppm.

2.8. Statistical analysis

Data are expressed as the mean ± standard deviation of three independent measurements unless otherwise stated. Statistical significance was evaluated by analysis of variance followed by Tukey's multiple-comparison test. For datasets involving both intervention temperature and ultrasound treatment, two-way ANOVA was used to evaluate the main effects and their interaction. When a significant interaction was observed, simple-effects comparisons were performed. Differences were considered significant at $p < 0.05$. Statistical analyses were conducted using SPSS version 29.0 (IBM Corp., Armonk, NY, USA), and figures were prepared using Origin 2023b (OriginLab Corp., Northampton, MA, USA).

3. Results and discussion

3.1. Morphological changes in hydrated and freeze-dried starch

3.1.1. Morphology of hydrated starch structures

CLSM was used to visualize the spatial distribution of FITC-associated fluorescent regions within hydrated starch systems (Fig. 1). Because FITC was not covalently conjugated with starch molecules in this study, the fluorescence signals were interpreted as qualitative indicators of spatial heterogeneity within the hydrated starch matrix rather than direct molecular labeling of starch components.

In the NCG groups (columns A and B), the overall dimensions of the ultrasound-treated structures are similar to those of the corresponding non-ultrasound controls, in agreement with the PSD results. However, the ultrasound-treated samples (columns B and D) showed more heterogeneous fluorescence distributions and variations in signal intensity, particularly at 69 °C (row 2) and 73 °C (row 3) [13]. At 60 °C, both NU-

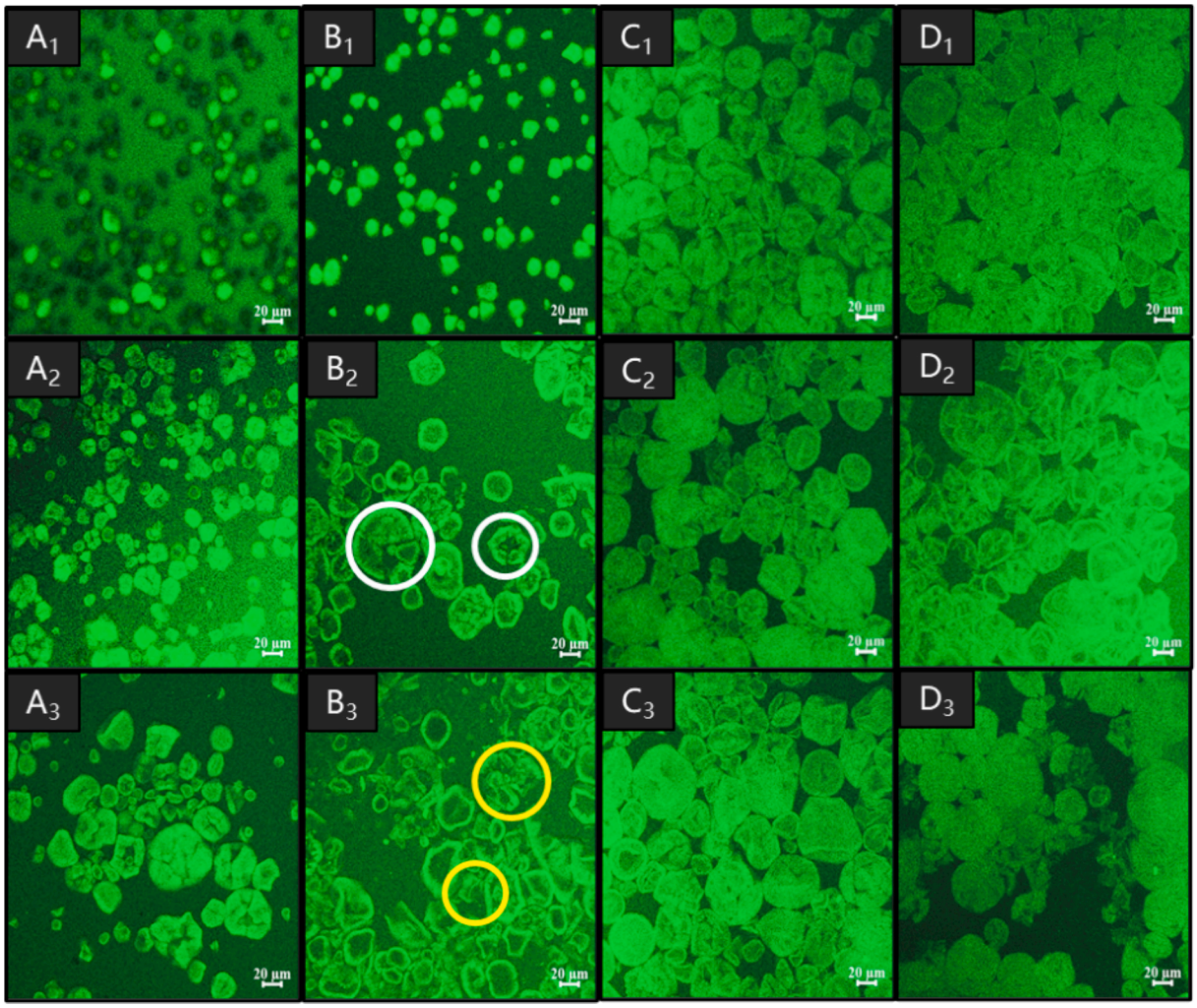


Fig. 1. Confocal laser scanning microscopy images of hydrated corn starch subjected to different treatments. Columns A–D correspond to NU-NCG, U-NCG, NU-CG, and U-CG, respectively; rows 1–3 correspond to intervention temperatures of 60, 69, and 73 °C, respectively. White and yellow circles mark representative regions of structural irregularity. Scale bar = 20 μm.

NCG (A1) and U-NCG (B1) showed recognizable granular structures, although slight differences in fluorescence distribution were observed. At 69 °C, the U-NCG (B2) sample exhibited more pronounced structural heterogeneity than the corresponding control (A2). At 73 °C, both thermal gelatinization and ultrasound contributed to substantial changes in the hydrated morphology, and the border of individual granules became less clear. After heating to 95 °C, the non-ultrasound-treated samples generally formed continuous swollen structures. The ultrasound-treated CG samples (column D) showed increasing heterogeneity with intervention temperature [14]. The difference was most apparent for 73-U-CG (D3), which displayed a less continuous and more fragmented appearance than 73-NU-CG (C3). These observations suggest that ultrasound influenced the spatial distribution and apparent heterogeneity of hydrated starch matrices under the applied treatment conditions, and this modification effect became more evident when ultrasound treatment was applied within the gelatinization range [22].

3.1.2. Surface morphology of freeze-dried samples

SEM images revealed clear stage-dependent differences in the morphology of the freeze-dried starch samples (Fig. 2). Samples treated at 60 °C retained the distinct polyhedral and oval granular morphology characteristic of native corn starch [23]. After ultrasound treatment, the granule surfaces became rougher, with small pits and depressions visible on otherwise intact granules (B_1). These results suggest that sonication at 60 °C mainly induced surface-level damage without extensive collapse of the granular structure. At 69 °C, the granules became more swollen and partially disrupted, and the ultrasound-treated sample showed more distinct pore-like openings and fissures on the granule surface (B_2). This result suggests that acoustic cavitation promoted surface erosion and localized rupture when the granules were hydrated and softened. At 73 °C, the granules exhibited extensive morphological degradation, with intact granules largely replaced by cracked, folded, and collapsed fragments. The marked region in Fig. 2B_3 further shows fragmented and ruptured starch structures, indicating that ultrasound near the gelatinization peak intensified the breakdown of softened granules. After complete gelatinization, the CG samples displayed larger collapsed sheets and porous matrix-like structures, especially in the 73-U-CG sample, where extensive fragmentation and honeycomb-like pores were observed.

CLSM results indicated that ultrasound-treated granules maintained an expanded outline in the hydrated state, whereas SEM revealed substantial collapse after freeze drying. This difference suggests that the starch granules may have had adequate volumetric support in the hydrated state but lower resistance to water removal and drying stress [24]. Therefore, the collapsed morphology in the freeze-dried samples reflects a combination of treatment-induced weakening and secondary deformation during sample preparation [25]. Overall, the CLSM and SEM results demonstrate that ultrasound-induced morphological changes depended on the gelatinization stage. Ultrasound applied before or at the onset of gelatinization introduced localized structural heterogeneity without destroying the bulk granular framework. Ultrasound intervention approaching the peak gelatinization temperature severely compromised network continuity and induced extensive structural collapse [26].

3.2. Rheological properties of gelatinized starch pastes

All completely gelatinized starch pastes exhibited shear-thinning behavior [27,28], as indicated by a continuous decrease in apparent viscosity with increasing shear rate (Fig. 3). The Herschel–Bulkley model fitted the flow curves well, with R^2 values greater than 0.99. Two-way ANOVA was conducted to investigate the interaction effects between intervention temperature and ultrasound treatment for the Herschel–Bulkley parameters (K, n) and hysteresis-loop area. At 60 °C, ultrasound did not significantly alter the K or n values in either the upward or downward shear rate tests, indicating comparable steady-flow behavior between 60-U-CG and 60-NU-CG. However, the hysteresis-loop area of 60-U-CG was significantly higher than that of 60-NU-CG ($p < 0.001$), suggesting more pronounced thixotropic behavior during the shear cycle, although the fitted K was not significantly increased. At 69 °C, ultrasound markedly reduced the K and increased n in both shear phases ($p < 0.001$), indicating lower flow resistance and a

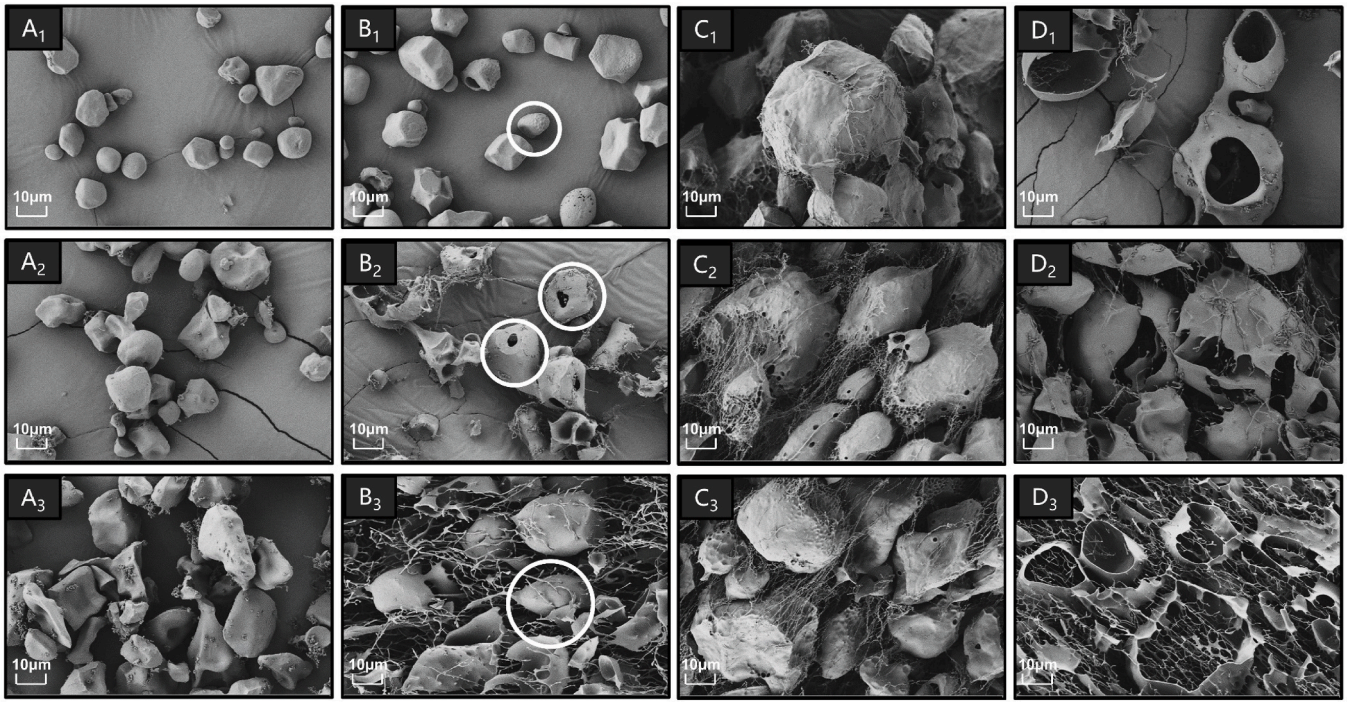


Fig. 2. Scanning electron microscopy images of freeze-dried corn starch subjected to different treatments. Columns A–D correspond to NU-NCG, U-NCG, NU-CG, and U-CG, respectively; rows 1–3 correspond to intervention temperatures of 60, 69, and 73 °C, respectively. Yellow circles mark representative surface depressions or pores. Scale bar = 10 μm.

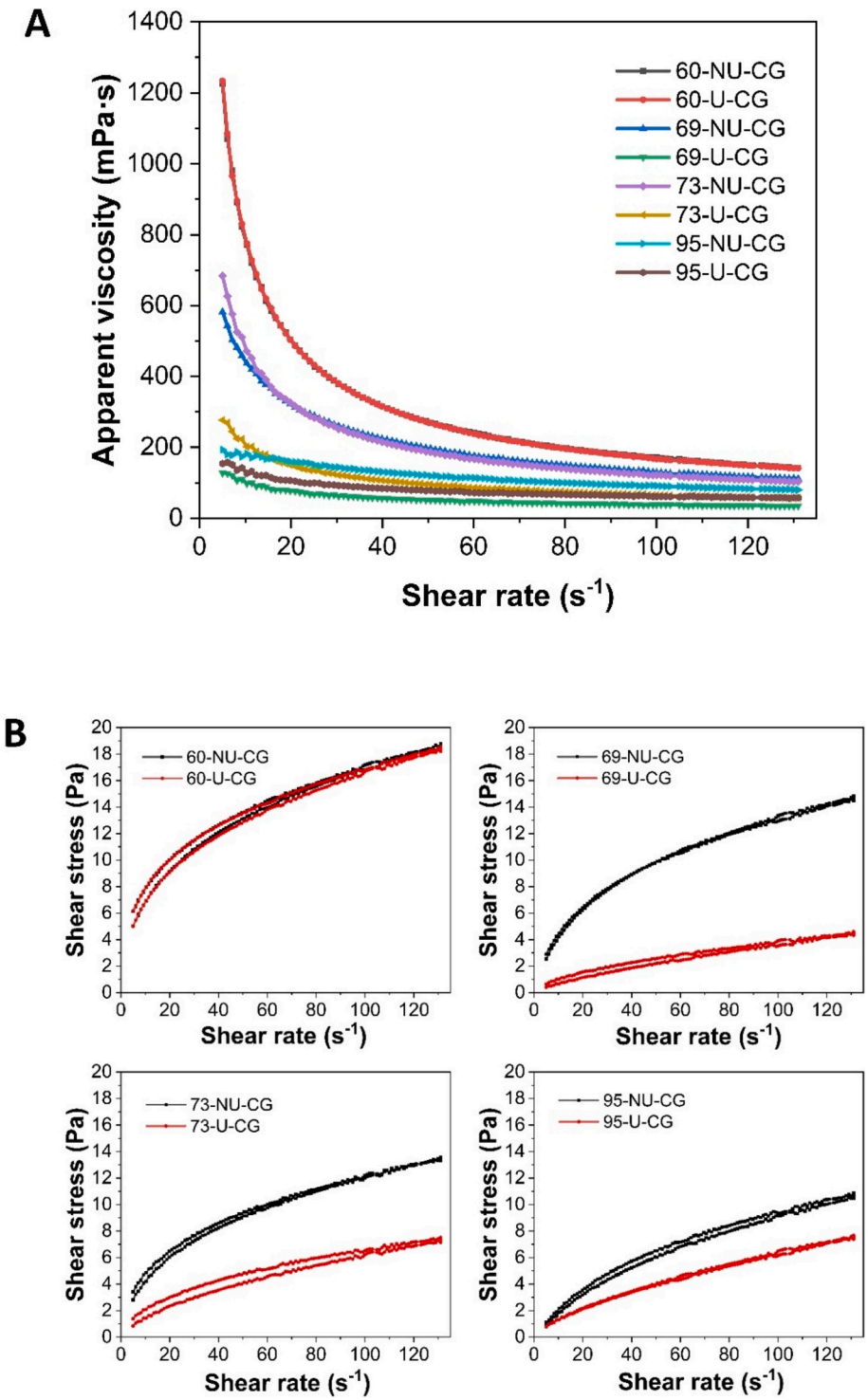


Fig. 3. Steady-shear rheological behavior of completely gelatinized corn starch pastes. (A) Apparent viscosity as a function of shear rate; (B) shear stress during upward and downward shear-rate sweeps at intervention temperatures of 60, 69, 73, and 95 °C.

shift toward Newtonian flow behavior compared with the corresponding non-ultrasound control [27]. The hysteresis-loop area also increased after ultrasound treatment, suggesting greater shear-induced breakdown and incomplete structural recovery during the downward shear test. A similar reduction in paste consistency was observed at 73 °C, where ultrasound significantly decreased K and increased n in both shear phases ($p < 0.001$). The increased hysteresis-loop area further indicated that the weakened paste network was more susceptible to structural rearrangement during the shear cycle. At 95 °C, ultrasound also reduced the K and increased n. Unlike the samples treated at 60–73 °C, the hysteresis-loop area decreased from 48.3 to 13.6 $Pa{\cdot}s^{-1}$ after ultrasound treatment at 95 °C ($p < 0.001$), suggesting that the terminally heated and sonicated paste contained fewer recoverable network structures and therefore exhibited weaker thixotropic behavior [15]. These results indicate that ultrasound-induced changes in paste consistency and viscoelastic properties depended on the intervention temperature [14,29]. Ultrasound applied at 60 °C mainly preserved the steady-flow parameters, whereas treatment at 69 and 73 °C reduced

paste consistency and viscoelastic strength. Treatment at 95 °C produced a low-consistency paste with a comparatively small hysteresis-loop area, indicating that ultrasound irreversibly disrupted swollen and fully gelatinized starch systems.

The frequency-sweep measurements further supported the stage-dependent changes in the viscoelastic behavior of the completely gelatinized pastes (Fig. 4). Although deviations were observed at the highest angular frequencies, these regions were not considered for interpretation because they may be affected by measurement artifacts. Therefore, the viscoelastic behavior was discussed based on the artifact-free frequency region (0.1–80 rad/s). At 60 °C, both 60-NU-CG and 60-U-CG maintained relatively high elastic moduli at low frequency. At 0.1 rad/s, G′ was 68.47 Pa for 60-NU-CG and 86.99 Pa for 60-U-CG, while G″ was much lower, at 11.95 and 17.40 Pa, respectively. As the angular frequency increased, the G′ values of the two samples converged: at 1 rad/s, G′ was 29.18 and 29.23 Pa for 60-NU-CG and 60-U-CG, respectively, and at 10 rad/s, the corresponding values were 17.28 and 16.51 Pa. This indicates that ultrasound intervention before the main gelatinization range did not weaken the final viscoelastic network. At 69 °C, ultrasound mainly reduced the intermediate-frequency G′. The G′ values of 69-NU-CG and 69-U-CG were similar at 0.1 rad/s, 18.13 and 18.66 Pa, respectively, but decreased from 2.89 to 0.54 Pa at 1 rad/s and from 1.03 to 0.27 Pa at 10 rad/s after ultrasound treatment. In comparison, the change in G″ was less pronounced, especially at 10 rad/s. At 73 °C, ultrasound also reduced both the storage and loss moduli of the final paste. G′ decreased from 38.58 to 30.30 Pa at 0.1 rad/s and from 11.76 to 3.77 Pa at 1 rad/s, while G″ decreased from 11.10 to 2.96 Pa and from 3.11 to 0.51 Pa at the same frequencies, respectively. The 95 °C groups served as fully gelatinized references. Their low intermediate-frequency moduli, together with the decrease in G′ from 3.47 to 1.67 Pa at 1 rad/s after ultrasound treatment, indicate that sonication of an already gelatinized paste reduced elastic strength [15,30,31]. Overall, the dynamic rheological data indicate that ultrasound applied at 60 °C largely preserved the elastic character of the final paste, whereas intervention at 69 and 73 °C reduced the intermediate-frequency elastic modulus to different extents. This result supports the steady-shear results, showing that ultrasound introduced during the gelatinization transition had a greater effect on the development of the final paste network than ultrasound applied before the main gelatinization range [29,32].

3.3. The hydration, swelling, and iodine-binding behavior of starch

3.3.1. Apparent particle-size distribution and swelling power

The NCG samples showed a dominant particle-size population centered at approximately 2.5 μm (Fig. 5). At each intervention temperature, the apparent particle-size distributions of ultrasound-treated and non-ultrasound-treated samples were similar, suggesting that ultrasound treatment did not cause substantial changes in the dispersed hydrated starch structures under the measurement conditions [13]. After final heating to 95 °C, the apparent particle-size distributions shifted toward larger hydrated structures, mainly within the range of 30–60 μm, reflecting extensive swelling and paste formation during complete gelatinization. Two-way ANOVA showed a significant interaction effect between intervention temperature and ultrasound treatment for the swelling power of the NCG samples ($p < 0.001$), indicating that the ultrasound-induced change in swelling power varied with the intervention temperature [22]. At 60 °C, ultrasound increased the swelling power from 3.7 to 5.8 g/g ($p < 0.01$). A further increase was observed at 69 °C, from 7.9 to 10.4 g/g ($p < 0.001$). In contrast, the difference between 73-U-NCG and 73-NU-NCG was not statistically significant. Within the NU series, swelling power increased progressively as the intervention temperature increased. Within the ultrasound

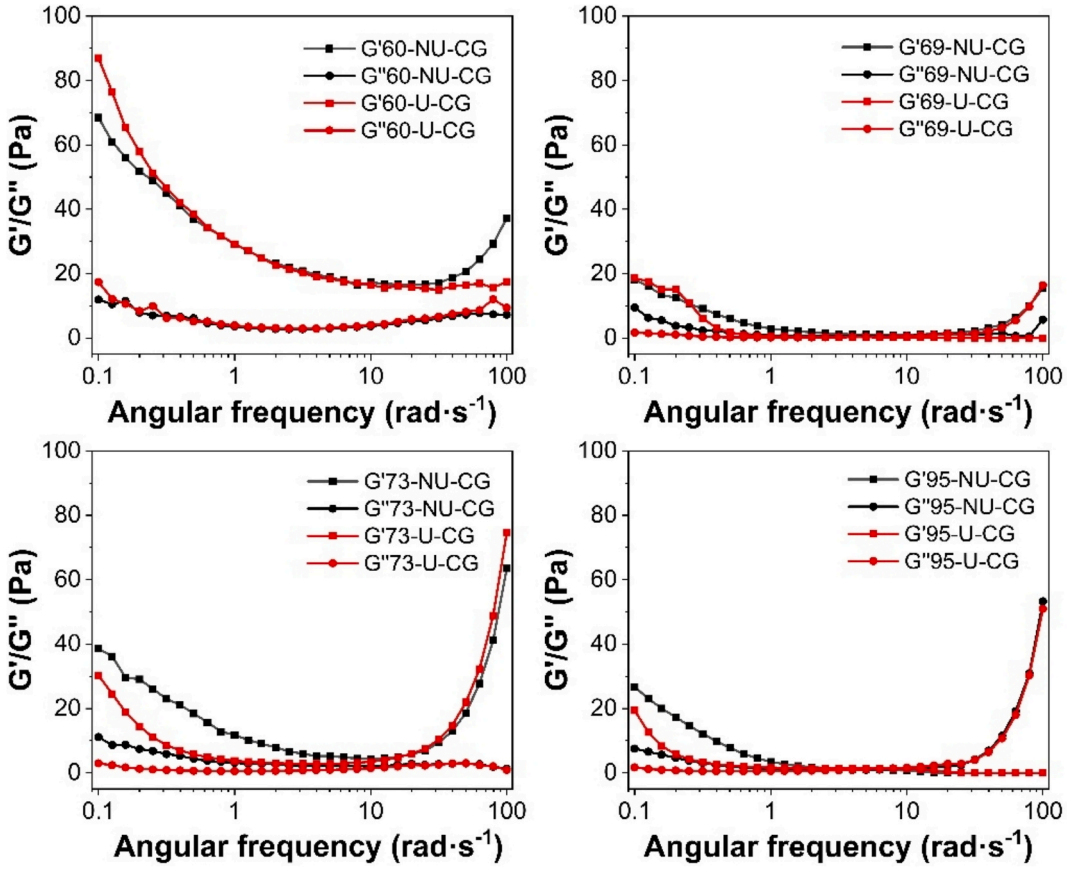


Fig. 4. Dynamic viscoelastic properties of completely gelatinized corn starch gels. Storage modulus (G′) and loss modulus (G″) are plotted as functions of angular frequency at 25 °C. The panels correspond to intervention temperatures of 60, 69, 73, and 95 °C.

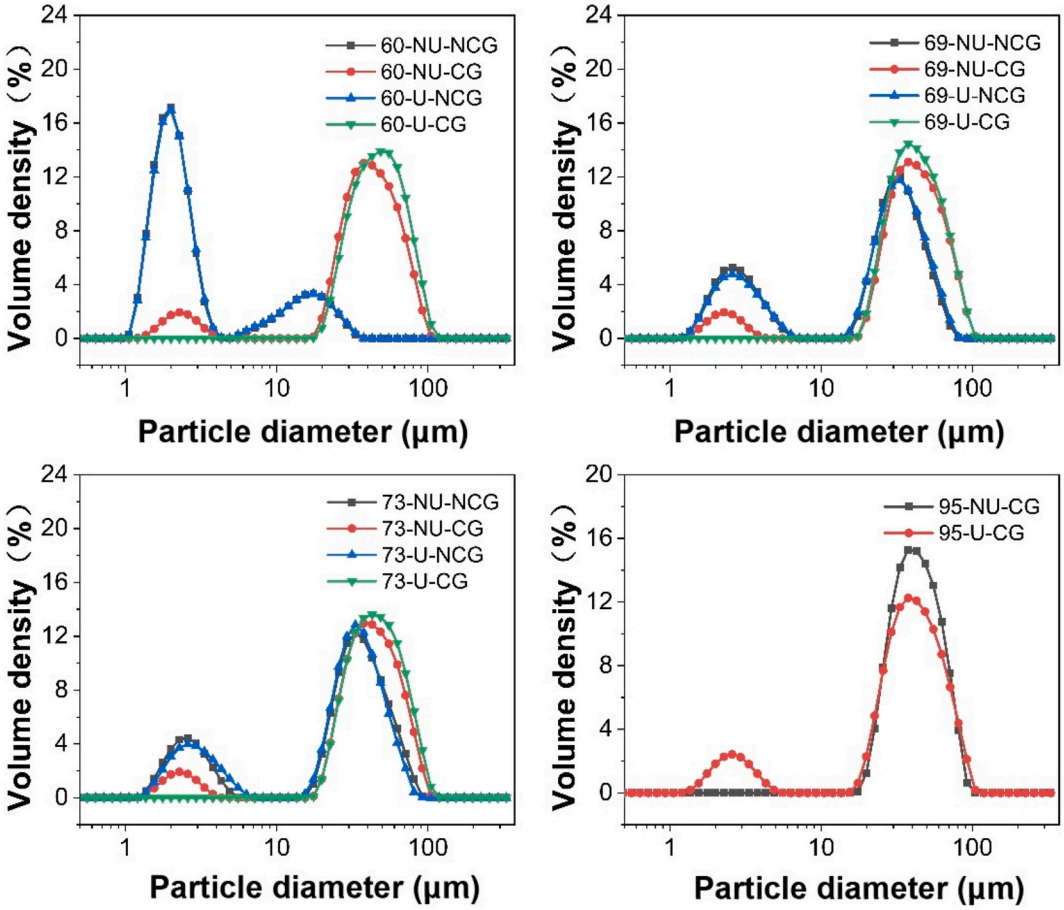


Fig. 5. Volume-based particle-size distributions of corn starch subjected to different treatment conditions. NCG and CG denote samples collected immediately after intervention and after subsequent heating to 95 °C, respectively.

treated groups, the highest value was observed at 69 °C, followed by 73 and 60 °C. Quantitative particle-size parameters (D10, D50, D90, D [2,3], and D [3,4]) are summarized in Supplementary Table 2. Statistical analysis indicated that ultrasound treatment had limited effects on the apparent particle-size distribution of NCG samples, whereas differences were more evident after complete gelatinization, particularly for volume-related parameters. These results suggest that ultrasound mainly influenced hydration and internal structural organization rather than directly causing extensive fragmentation of starch granules. It should be noted that laser diffraction measurements require dilution and dispersion of gelatinized starch samples in deionized water. Therefore, weakly associated hydrated aggregates may be partially disrupted during sample preparation and measurement, and the obtained values should be interpreted as apparent particle-size distributions rather than the intact size of hydrated starch assemblies.

A significant interaction effect between intervention temperature and ultrasound treatment was also detected for the swelling power of the CG samples ($p = 0.012$). Ultrasound increased the final swelling power when applied at 60 °C ($p < 0.001$) and 69 °C ($p < 0.01$), whereas no significant difference was observed between 73-U-CG and 73-NU-CG. Among the non-ultrasound-treated CG samples, swelling power did not differ significantly across the three intervention temperatures. Among the ultrasound-treated samples, 60-U-CG had a higher swelling power than 69-U-CG and 73-U-CG, whereas the latter two groups were

Table 2
Herschel–Bulkley parameters and thixotropic hysteresis areas of completely gelatinized corn starch pastes.

Sample	Upward curve (Structure)			Downward curve (Flow)			Thixotropy
	σ_0 (Pa)	K (Pa·s^n)	n (−)	σ_0 (Pa)	K (Pa·s^n)	n (−)	Area (Pa·s^{-1})
60-NU-CG	0.00 ± 0.20 ^{a}	3.69 ± 0.13 ^{a}	0.33 ± 0.01 ^{d}	0.00 ± 0.26 ^{a}	2.96 ± 0.16 ^{a}	0.38 ± 0.01^{c}	51.5 ± 1.2 ^{a}
60-U-CG	0.00 ± 0.21 ^{a}	3.78 ± 0.14 ^{a}	0.33 ± 0.01 ^{d}	0.00 ± 0.20 ^{a}	2.95 ± 0.12 ^{a}	0.37 ± 0.01 ^{d}	69.8 ± 1.9 ^{a***}
69-NU-CG	0.00 ± 0.29 ^{a}	1.77 ± 0.15^{b}	0.43 ± 0.01^{b}	0.00 ± 0.34 ^{a}	1.61 ± 0.17^{b}	0.46 ± 0.02^{b}	5.6 ± 0.4 ^{d}
69-U-CG	0.04 ± 0.05 ^{a}	0.26 ± 0.02^{c***}	0.58 ± 0.01^{b***}	0.01 ± 0.04 ^{a}	0.12 ± 0.01^{c***}	0.73 ± 0.01 ^{a***}	36.4 ± 0.9^{b***}
73-NU-CG	0.00 ± 0.20 ^{a}	2.01 ± 0.12^{b}	0.39 ± 0.01^{c}	0.00 ± 0.23 ^{a}	1.66 ± 0.12^{b}	0.43 ± 0.01^{b}	30.4 ± 0.7^{c}
73-U-CG	0.00 ± 0.10 ^{a}	0.72 ± 0.05^{b***}	0.48 ± 0.01^{c***}	0.00 ± 0.06 ^{a}	0.37 ± 0.02^{b***}	0.61 ± 0.01^{c***}	68.2 ± 1.7 ^{a***}
95-NU-CG	0.00 ± 0.16 ^{a}	0.53 ± 0.05^{c}	0.62 ± 0.02 ^{a}	0.00 ± 0.22 ^{a}	0.71 ± 0.08^{c}	0.56 ± 0.02 ^{a}	48.3 ± 1.5^{b}
95-U-CG	0.03 ± 0.04 ^{a}	0.27 ± 0.01^{c*}	0.68 ± 0.01 ^{a***}	0.00 ± 0.05 ^{a}	0.29 ± 0.01^{b***}	0.67 ± 0.01^{b***}	13.6 ± 0.8^{c***}

Values are expressed as the mean ± standard deviation (n = 3). Within each ultrasound condition (NU or U), different lowercase letters in the same column indicate significant differences among intervention temperatures according to Tukey's multiple-comparison test ($p < 0.05$). Asterisks indicate significant differences between U and NU samples at the same intervention temperature based on simple-effects comparisons following two-way ANOVA: *$p < 0.05$, **$p < 0.01$, and ***$p < 0.001$. σ_0, yield stress; K, consistency index; n, flow behavior index.

statistically comparable [33,34]. These results indicate that the ultrasound-induced enhancement of water uptake was most evident before and near the onset of gelatinization. When ultrasound was applied near the gelatinization peak, extensive thermal hydration and structural disordering had already occurred, and the additional contribution of ultrasound to swelling became limited. The similar apparent particle-size distributions observed in NCG samples together with the altered swelling power of CG samples suggest that ultrasound influenced hydration-related properties without necessarily causing extensive fragmentation of dispersed hydrated starch structures under the measurement conditions. Surface roughening, weakened intermolecular associations, or increased granule permeability could have contributed to this result [14].

3.3.2. Iodine-reactive soluble starch release and iodine-binding characteristics

The iodine-reactive amylose-equivalent concentration showed a significant interaction effect between intervention temperature and ultrasound treatment in both the NCG and CG datasets ($p < 0.001$), indicating that the effect of ultrasound changed as gelatinization progressed [22]. For the NCG samples, ultrasound increased the iodine-reactive signal at 60 °C, from 194 to 378 μg/mL ($p < 0.001$). In contrast, ultrasound reduced the corresponding signal at 69 °C, from 1735 to 884 μg/mL, and at 73 °C, from 2299 to 685 μg/mL (both $p < 0.001$). Within the NU series, the iodine-reactive concentration increased progressively from 60 to 73 °C. Within the U series, the highest value occurred at 69 °C, followed by 73 and 60 °C. These stage-dependent changes indicate that ultrasound altered the iodine-reactive soluble starch fractions and their iodine-binding responses differently at the three intervention temperatures. For the CG samples, all ultrasound-treated groups showed lower iodine-reactive amylose-equivalent concentrations than their corresponding non-ultrasound controls. The decrease was significant at 60 °C ($p < 0.01$) and more pronounced at 69 and 73 °C ($p < 0.001$). Within the NU series, the values at 69 and 73 °C were statistically comparable and both exceeded that at 60 °C. Within the U series, the value was highest for 69-U-CG, intermediate for 60-U-CG, and lowest for 73-U-CG.

The full-wavelength absorption spectra were used to further examine the iodine-binding behavior of soluble starch fractions in the supernatants (Fig. 6). The starch–iodine complexes exhibited similar absorption profiles, with λmax values ranging from 612 to 623 nm. This demonstrates that ultrasonic intervention did not fundamentally alter the primary absorption characteristics of the starch–iodine complexes [35]. In contrast, the absorption intensity changed more clearly among treatments, consistent with the iodine-reactive amylose-equivalent concentrations shown in Table 3. In the NCG samples, ultrasound increased the iodine-reactive concentration at 60 °C but decreased it at 69 and 73 °C. In the CG samples, ultrasound generally reduced the iodine-reactive concentration, with the largest decrease observed at 73 °C. These results indicate that ultrasound mainly changed the amount of iodine-reactive soluble starch fractions, while the dominant iodine-binding spectral region remained similar. Overall, sonication at 60 °C increased the iodine-reactive soluble starch fraction, whereas treatment within the onset-to-peak transition reduced the detectable iodine-reactive fraction under the applied conditions [14].

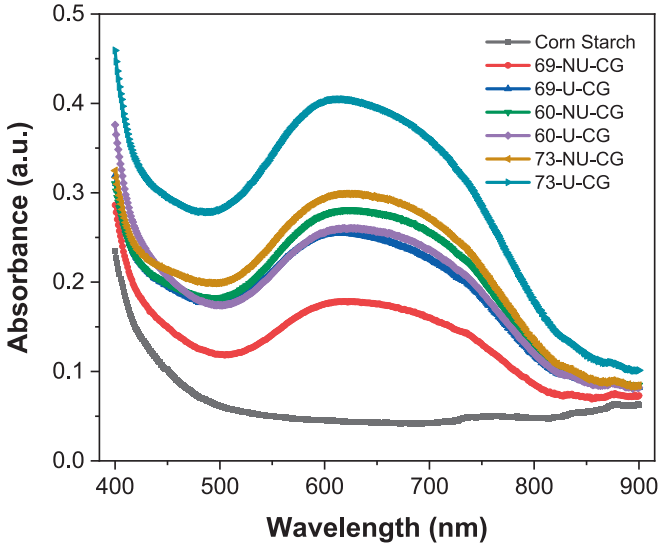


Fig. 6. UV–visible absorption spectra of starch–iodine complexes formed with soluble starch in corn starch supernatants.

3.4. Changes in crystalline order, short-range molecular organization, and apparent molecular-weight distribution

3.4.1. Long-range crystalline order

The 60 °C NCG samples retained the characteristic X-ray diffraction features of nanocrystals with an orthorhombic crystal structure, consistent with the A-type classification of corn starch (Fig. 7). Second-derivative analysis identified the principal diffraction regions at approximately 15.0°, 17.0°, 17.9–18.0°, 20.0°, and 22.8–22.9° (2θ). Because several orthorhombic reflections occur at closely spaced Bragg angles and overlap within the relatively broad diffraction features of starch, these regions were assigned to composite reflections corresponding mainly to (121)/(200), (130)/(031), (211)/(220), (040), and (231)/(310)/(132), respectively.

The corresponding peak positions differed by only 0.02–0.06° between 60-NU-NCG and 60-U-NCG, with both samples showing the same principal composite reflection assignments. These results indicate that the characteristic orthorhombic diffraction features were largely retained after ultrasound treatment at 60 °C, with no apparent transformation of the detectable crystalline phase. However, the preservation of peak positions and Miller-index assignments does not exclude local molecular rearrangement or partial disruption of ordered domains that

Table 3
Swelling power and iodine-reactive amylose-equivalent concentration of corn starch under different treatment conditions.

NCG Sample	Swelling power (g/g)	Iodine-reactive amylose-equivalent concentration (μg/mL)	CG Sample	Swelling power (g/g)	Iodine-reactive amylose-equivalent concentration (μg/mL)
60-NU-NCG	3.7 ± 0.2^{c}	194 ± 2^{c}	60-NU-CG	10.5 ± 0.4^{a}	2218 ± 21^{b}
60-U-NCG	$5.8 \pm 0.3^{c**}$	$378 \pm 4^{c***}$	60-U-CG	$13.4 \pm 0.8^{a***}$	$2030 \pm 26^{b**}$
69-NU-NCG	7.9 ± 0.6^{b}	1735 ± 16^{b}	69-NU-CG	9.59 ± 0.4^{a}	3298 ± 79^{a}
69-U-NCG	$10.4 \pm 0.9^{a***}$	$884 \pm 12^{a***}$	69-U-CG	$11.6 \pm 1.0^{b**}$	$2377 \pm 23^{a***}$
73-NU-NCG	9.5 ± 0.4^{a}	2299 ± 39^{a}	73-NU-CG	10.7 ± 0.1^{a}	3405 ± 81^{a}
73-U-NCG	8.7 ± 0.7^{b}	$685 \pm 19^{b***}$	73-U-CG	10.9 ± 0.8^{b}	$1072 \pm 24^{c***}$

Values are expressed as the mean ± standard deviation (n = 3). The NCG and CG datasets were analyzed separately using two-way ANOVA, with intervention temperature and ultrasound treatment as fixed factors. Within each sample state and ultrasound condition, different lowercase letters in the same column indicate significant differences among intervention temperatures according to Tukey's multiple-comparison test ($p < 0.05$). Asterisks indicate significant differences between ultrasound-treated and non-ultrasound-treated samples at the same intervention temperature based on simple-effects comparisons with Bonferroni adjustment: *$p < 0.05$, **$p < 0.01$, and ***$p < 0.001$. The lowercase letters assigned to the NU and U series represent separate temperature comparisons and should not be compared directly across ultrasound conditions.

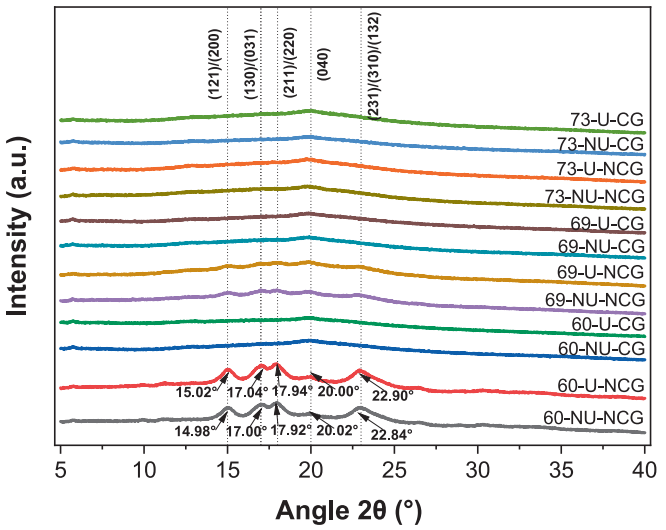


Fig. 7. X-ray diffraction patterns of corn starch subjected to thermal and ultrasonic treatments at different intervention temperatures. Peak positions associated with orthorhombic nanocrystalline organization characteristic of A-type corn starch were identified using second-derivative analysis (Supplementary Fig. S1).

retains the overall crystallographic organization [11].

At 69 °C, residual diffraction features remained within the regions corresponding to the principal orthorhombic reflections, but they became substantially broader and less resolved, particularly in 69-U-NCG. The persistence of these features alongside their broadening is consistent with partial disruption of crystalline organization as the starch approached the main gelatinization transition. Comparable reductions in structural order have been reported following hydrodynamic-cavitation treatment, with responses depending on botanical origin and treatment conditions [36,37]. In hydrothermally treated high-amylose maize starch, SAXS revealed disruption of semi-crystalline lamellar regularity, while XRD indicated a decrease in relative crystallinity [38]. By analogy, hydration and swelling may have disturbed the organization of nanocrystalline domains within the lamellar architecture in the present samples. However, lamellar disruption remains a proposed mechanism because lamellar periodicity was not measured directly. Reduced crystalline perfection may also contribute to the less resolved diffraction features, although peak broadening alone cannot distinguish lattice disorder from changes in coherent domain size and overlapping reflections. Consequently, the profiles at 69 °C were interpreted qualitatively rather than as evidence of specific crystal-plane transformations.

Samples treated at 73 °C, as well as most CG samples, exhibited predominantly diffuse diffraction profiles without clearly resolved reflections characteristic of the native orthorhombic nanocrystalline structure. These results indicate a pronounced loss of detectable long-range crystalline order following intervention near the gelatinization peak or subsequent heating to 95 °C. No additional well-resolved reflections attributable to another crystalline phase were observed. Nevertheless, the absence of new reflections does not exclude reorganization within the same crystalline phase or limited chain reassociation during cooling [39]. Previous research reported that sonicated high-amylose corn starch developed stronger diffraction features and increased relative crystallinity during subsequent retrogradation, demonstrating that ultrasound-induced disruption can be followed by recrystallization under suitable storage conditions [40]. In contrast, the predominantly diffuse profiles observed here indicate that substantial long-range crystalline order was not recovered to a clearly detectable extent under the applied sample preparation conditions. Because XRD was performed on recovered samples, the respective contributions of disruption during heating and reorganization during cooling cannot be separated [41].

Overall, the XRD results reveal an intervention-stage-dependent evolution of crystalline organization: orthorhombic nanocrystalline diffraction features were largely retained at 60 °C, became broader and less distinct at 69 °C, and were no longer clearly resolved after intervention near the gelatinization peak or subsequent heating to 95 °C. These observations support progressive disruption of long-range crystalline organization, potentially accompanied by perturbation of the lamellar architecture and limited molecular reorganization during cooling. The latter processes remain mechanistic interpretations rather than independently established structural changes. Their relationship with the FTIR-derived indicators of local molecular organization is discussed below.

3.4.2. *Short-range molecular organization*

Solid-state ^{13}C CP/MAS NMR was used to examine changes in the short-range molecular environments of the starch samples (Fig. 8). All spectra showed typical starch carbon signals, including the C1 region at 98–103 ppm, the C4 region at 80–84 ppm, the C2/C3/C5 region at 70–78 ppm, and the C6 region at 60–64 ppm. The 60-NU-NCG and 60-U-NCG samples showed similar C1 resonance profiles, characterized by a primary signal near 100 ppm and distinctly resolved shoulders in the 98–103 ppm region. This suggests that ultrasound treatment at 60 °C caused limited changes in the local molecular environments reflected by the C1 spectral region before the main gelatinization transition [42]. This observation is consistent with the preservation of characteristic orthorhombic nanocrystalline diffraction features in the 60 °C XRD profiles [43]. The C1 resonance was broader and less clearly resolved in samples treated within the gelatinization range, particularly 69-U-NCG and the 73 °C groups, as well as in the CG samples [44]. The reduced resolution and broader C1 signal indicate changes in the distribution of local molecular environments within starch. Such spectral changes may reflect alterations in local molecular organization during gelatinization; however, they cannot be directly interpreted as quantitative changes in ordered or disordered fractions. Spectral variations in the C4 and C6 regions further suggest changes in the local chemical environments associated with glycosidic linkages and hydroxymethyl carbons after thermo-ultrasonic treatment [45]. Thus, the NMR results provide complementary evidence to DSC and XRD analyses by indicating that ultrasound applied within the gelatinization range was associated with

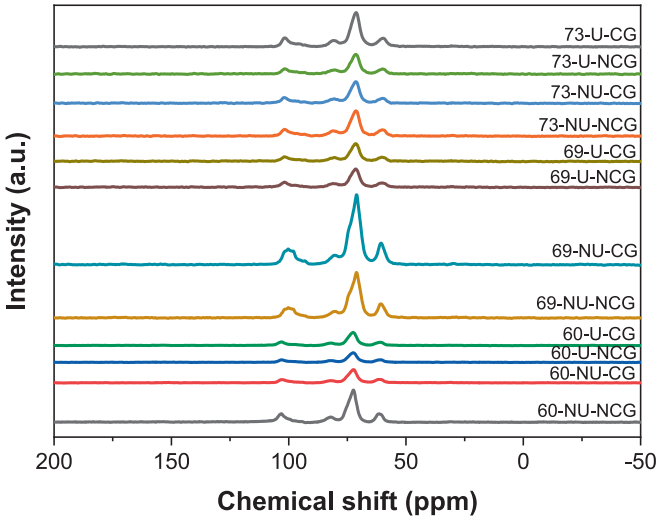


Fig. 8. Solid-state ^{13}C CP/MAS NMR spectra of corn starch subjected to thermal and ultrasonic treatments at 60, 69, and 73 °C. Major resonance regions are assigned to C1 (98–103 ppm), C4 (80–84 ppm), C2/C3/C5 (70–78 ppm), and C6 (60–64 ppm).

changes in starch spectral profiles, whereas treatment at 60 °C largely preserved the characteristic C1 spectral features [46].

3.4.3. Apparent molecular-weight profiles

The GPC analysis revealed apparent differences in the pullulan-equivalent molecular-size distribution of the DMSO/LiBr-soluble starch fractions among different thermo-ultrasonic treatments (Table 4). For NCG samples, ultrasound treatment resulted in variations in apparent molecular-size parameters depending on the intervention temperature. At 60 °C, Mw increased from 3.37 × 10^7 to 5.69 × 10^7, whereas Mz increased from 6.42 × 10^8 to 1.94 × 10^9. At 69 °C, Mw showed only a slight variation (6.32 × 10^7 to 6.79 × 10^7), while Mz increased from 1.97 × 10^9 to 4.11 × 10^9. At 73 °C, the apparent molecular-size parameters also showed changes after ultrasound treatment, including increases in Mw and Mp. For CG samples, ultrasound treatment resulted in different changes in apparent molecular-size parameters depending on the intervention temperature. The observed variations in Mw, Mz, and Mp did not follow a consistent trend, suggesting that thermo-ultrasonic treatment did not produce a uniform change in the apparent molecular-size distribution under the investigated conditions [47–49].

The analysis was based on a single chromatographic measurement, and starch molecular-size determination using DMSO/LiBr dissolution may be affected by incomplete dissolution, molecular association, aggregation behavior, filtration efficiency, and the contribution of high-molecular-weight fractions. Therefore, the observed variations should not be interpreted as direct evidence of molecular chain degradation or molecular growth. Instead, the GPC results provide preliminary information regarding differences in the apparent molecular-size distribution of soluble starch fractions after thermo-ultrasonic treatment. Because the hydrodynamic properties of highly branched amylopectin differ from those of the pullulan calibration standards, the measured values should be interpreted as apparent molecular-size parameters rather than absolute molecular weights [50–52].

Table 4
Pullulan-equivalent apparent molecular-weight parameters of corn starch after thermal and ultrasound treatments.

Sample	M_n (×10^6)	M_w (×10^6)	M_p (×10^6)	M_z (×10^6)	M_w/M_n	M_z/M_w
60-NU-NCG	3.3	33.7	14.3	641.6	10.18	19.05
60-U-NCG	2.7	56.9	16.0	1938.8	20.86	34.08
60-NU-CG	2.6	79.4	44.2	9603.7	30.87	120.93
60-U-CG	3.2	68.8	13.8	2032.2	21.42	29.55
69-NU-NCG	3.4	63.2	13.8	1973.4	18.67	31.21
69-U-NCG	2.9	67.9	13.8	4112.7	23.62	60.61
69-NU-CG	2.7	64.8	12.2	2127.0	24.12	32.80
69-U-CG	3.3	53.3	13.2	1872.0	16.37	35.14
73-NU-NCG	2.9	53.2	12.6	1829.7	18.49	34.41
73-U-NCG	3.6	62.0	44.8	3741.8	17.16	60.35
73-NU-CG	2.9	65.8	13.0	1744.2	22.80	26.50
73-U-CG	3.4	86.3	52.3	2359.8	25.63	27.34

M_n, number-average molecular weight; M_w, weight-average molecular weight; M_p, peak molecular weight; M_z, z-average molecular weight; M_w/M_n, polydispersity index; M_z/M_w, molecular-weight distribution width. Values were obtained by relative calibration against pullulan standards and represent single chromatographic analyses for each treatment condition.

3.5. FTIR spectral characteristics and temperature-dependent spectral coupling

3.5.1. FTIR spectral characteristics

The FTIR spectra of all starch samples retained the characteristic absorption profile of the starch matrix (Fig. 9). The broad envelope at approximately 3680–3000 cm^{-1} was mainly attributed to overlapping O–H stretching contributions from starch hydroxyl groups and associated water, reflecting sensitivity to both hydrogen-bonding environments and sample hydration. The band near 1640 cm^{-1} was primarily assigned to the H–O–H bending vibration of associated water, whereas the 1200–900 cm^{-1} fingerprint region contained overlapping C–O–C and C–O stretching vibrations of glucopyranose units that are sensitive to local starch organization. No additional absorption bands were detected after ultrasound treatment, providing no evidence of new chemical functionalities detectable by FTIR under the applied conditions. This contrasts with chemically esterified starch, for which new carbonyl absorption bands associated with ester-bond formation have been reported.

Although the O–H stretching region is sensitive to hydrogen bonding, no systematic shift of the broad envelope was resolved among treatments. The spectra therefore do not establish an overall strengthening or weakening of hydrogen bonding. Instead, changes in starch–starch and starch–water interactions accompanying hydration and molecular rearrangement offer a possible explanation for the treatment-dependent spectral variations [53]. This interpretation is consistent with the hydrogen-bond reorganization discussed for ultrasound-assisted starch hydrolysis, although the treatment systems differ. Because the present spectra were acquired from lyophilized samples, they characterize the recovered starch matrix and do not directly resolve the hydrogen-bond network during thermo-ultrasonic treatment [41].

Ultrasound treatment produced changes in the carbohydrate fingerprint region that depended on the intervention temperature. For the NCG samples, the 1047/1022 cm^{-1} ratio changed only slightly at 60 °C, from 0.900 to 0.902, whereas it increased from 0.868 to 0.886 at 69 °C and from 0.848 to 0.865 at 73 °C. For the CG samples, the corresponding ratio increased from 0.849 to 0.865 at 60 °C, from 0.878 to 0.913 at 69 °C, and from 0.830 to 0.904 at 73 °C. In contrast, the 995/1022 cm^{-1} ratio decreased after ultrasound treatment in the CG samples, particularly at 69 and 73 °C, from 1.242 to 1.166 and from 1.370 to

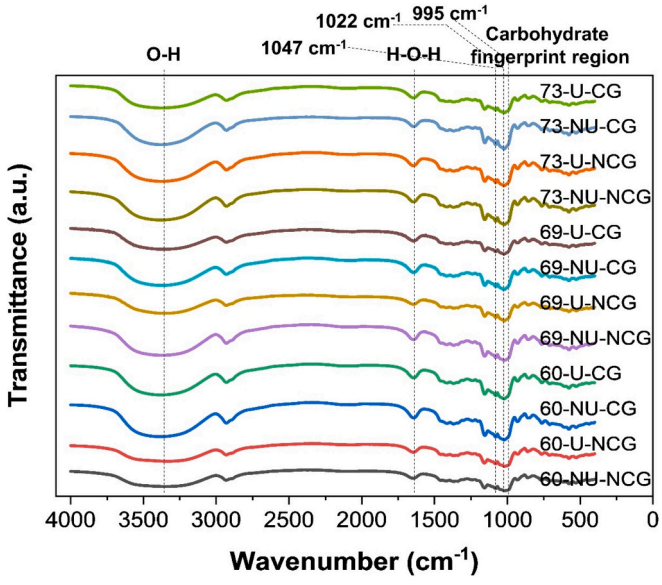


Fig. 9. FTIR spectra of corn starch subjected to thermal and ultrasonic treatments at 60, 69, and 73 °C. Major bands associated with O–H stretching, absorbed water, and carbohydrate-related vibrations are indicated.

1.151, respectively. These changes indicate redistribution of the relative vibrational contributions from different local molecular environments within the starch matrix.

Previous studies of modified starch have reported that decreases in the 1047/1022 cm^{-1} ratio can accompany disruption of molecular order and reductions in XRD-derived crystallinity. For example, hydrodynamic cavitation-assisted microbubble treatment decreased the 1047/1022 cm^{-1} ratio together with structural/crystalline order, whereas combined freezing–thawing and ultrasound-assisted enzymatic modification produced concurrent decreases in the 1047/1022 cm^{-1} ratio and relative crystallinity. In the present study, however, the 1047/1022 cm^{-1} ratio did not decrease in parallel with the pronounced weakening of the XRD diffraction features at 69 and 73 °C [36].

This divergence indicates that the FTIR band ratio and XRD probe different levels of starch organization. The 1047/1022 cm^{-1} ratio is therefore interpreted here as a comparative indicator of local molecular organization, whereas XRD reflects detectable long-range crystalline organization. Loss of long-range crystallographic coherence may coexist with local chain rearrangement, altered hydration, and redistribution of hydrogen-bonding environments. Accordingly, the increased 1047/1022 cm^{-1} ratios observed in some ultrasound-treated samples should not be interpreted as evidence of increased bulk crystallinity or recrystallization.

When considered together, the XRD and FTIR results indicate that thermo-ultrasonic treatment affected starch organization at different structural length scales. XRD primarily reflects detectable long-range crystalline organization, whereas the FTIR band ratios provide empirical information on changes in local molecular environments and short-range molecular organization. At 60 °C, the preservation of the principal orthorhombic diffraction features was accompanied by only a negligible change in the 1047/1022 cm^{-1} ratio in the NCG samples (0.900–0.902), indicating that long-range crystalline organization was largely retained while the local molecular environment changed only slightly under this early-stage intervention [54].

In contrast, at 69 and 73 °C, the marked broadening or disappearance of the characteristic XRD reflections indicated a substantial loss of detectable long-range crystalline order, whereas the 1047/1022 cm^{-1} ratio did not decrease correspondingly and, in several cases, increased after ultrasound treatment. This apparent divergence does not represent an inconsistency between the two techniques, because they probe different levels of starch organization. Loss of long-range crystallographic coherence may occur concurrently with local chain rearrangement, altered hydration, and redistribution of hydrogen-bonding environments, all of which can modify FTIR band ratios without restoring an extended crystalline lattice.

Accordingly, the increased 1047/1022 cm^{-1} ratios observed in some ultrasound-treated samples are more appropriately interpreted as changes in local molecular organization rather than as evidence of increased bulk crystallinity or recrystallization. Taken together, the XRD and FTIR results indicate that the structural response at the later intervention stages involved a pronounced loss of long-range crystalline organization accompanied by redistribution of local molecular interactions within the hydrated starch matrix.

3.5.2. Two-dimensional correlation spectroscopy

FTIR-based 2D-COS was used as a complementary analysis to compare temperature-dependent spectral variations among the NU-NCG, U-NCG, NU-CG, and U-CG series (Fig. 10). The synchronous maps showed correlated changes mainly in the O–H stretching region, the water-associated region, and the starch fingerprint region, consistent with results observed in the one-dimensional FTIR spectra [55]. However, the contour distributions differed among treatment groups. In the NU-NCG samples, the synchronous correlations were relatively broad, suggesting that heating from 60 to 73 °C produced coordinated spectral changes across several starch-related regions. In contrast, the U-NCG series showed more clearly resolved correlation features in the O–H stretching and fingerprint regions. This difference suggests that ultrasound modified the temperature-dependent spectral response of starch during the gelatinization transition, particularly in regions associated with hydroxyl-related vibrations and short-range structural organization. After subsequent heating to 95 °C, the synchronous maps of NU-CG and U-CG became more similar, particularly in the O–H stretching and water-associated regions. This convergence suggests that complete gelatinization diminished some of the spectral differences associated with the preceding ultrasound treatment. Nevertheless, residual variations remained detectable within the carbohydrate fingerprint region, indicating that the structural effects of the prior acoustic intervention were not completely overridden by subsequent terminal heating [56].

The asynchronous maps provided exploratory information about differences in the relative responses of spectral regions during thermo-ultrasonic intervention. Cross-bands involving the O–H stretching, water-associated, and starch fingerprint regions suggested that these spectral regions exhibited different response behaviors during thermo-ultrasonic intervention. However, due to the limited number of perturbation points, these asynchronous features should be interpreted as exploratory spectral responses rather than definitive evidence of sequential molecular changes [57–59]. The more distinct asynchronous features in the U-NCG series suggest that ultrasound influenced the relative spectral responses during the gelatinization transition. This interpretation is consistent with previous findings that starch FTIR bands are strongly influenced by hydration and short-range molecular organization, and that ultrasound-induced structural changes vary with treatment temperature [48,60].

3.6. DSC gelatinization properties

During heating, starch gelatinization represents a hierarchical structural transition rather than the melting of an individual starch component. It involves water uptake and swelling, progressive disruption of hydrated ordered structures, loss of detectable crystalline organization, and increased molecular mobility. Therefore, the DSC endothermic transition is interpreted here as the thermal response associated with disruption of hydrated ordered structures during gelatinization. The native corn starch exhibited an onset gelatinization temperature (T_o) of 69.11 °C, a peak temperature (T_p) of 73.00 °C, and a conclusion temperature (T_c) of 76.57 °C (Table 5). Based on the DSC-derived gelatinization transition region of native corn starch, 60, 69, and 73 °C were selected as representative intervention temperatures to investigate ultrasound effects at different positions along the gelatinization transition. A treatment temperature of 95 °C was included as a fully processed reference condition, where the absence of a detectable gelatinization transition was further verified by DSC analysis.

At 60 °C, NCG samples (60-NU-NCG and 60-U-NCG) exhibited detectable endothermic transition peaks (Fig. 11). Their T_o and T_p values were comparable, and the T_c values also showed no significant ultrasound-induced shift, indicating that ultrasound at 60 °C caused no significant shift in the gelatinization transition temperature. 60-U-NCG showed a higher ΔH (1.63 J/g) than 60-NU-NCG (1.38 J/g), although both values remained lower than that of native corn starch. This difference suggests that ultrasound treatment at 60 °C did not cause additional disruption of the remaining detectable ordered structures during the early gelatinization transition [61]. A weak thermal peak was visible for 60-U-CG at approximately 72–77 °C, which may be related to structural rearrangement during sample preparation before DSC analysis [62]. At 69 °C, only a weak endothermic transition was detected in 69-NU-NCG, with a ΔH of 0.15 J/g, whereas no detectable transition was observed for 69-U-NCG. This result indicates that ultrasound promoted the disruption of ordered structures in starch when applied near T_o [63]. No detectable endothermic transition was observed in the samples treated at 73 °C (both NCG and CG samples). This suggests that ultrasound intervention near the peak gelatinization transition resulted in substantial disruption of ordered structures, leaving no detectable

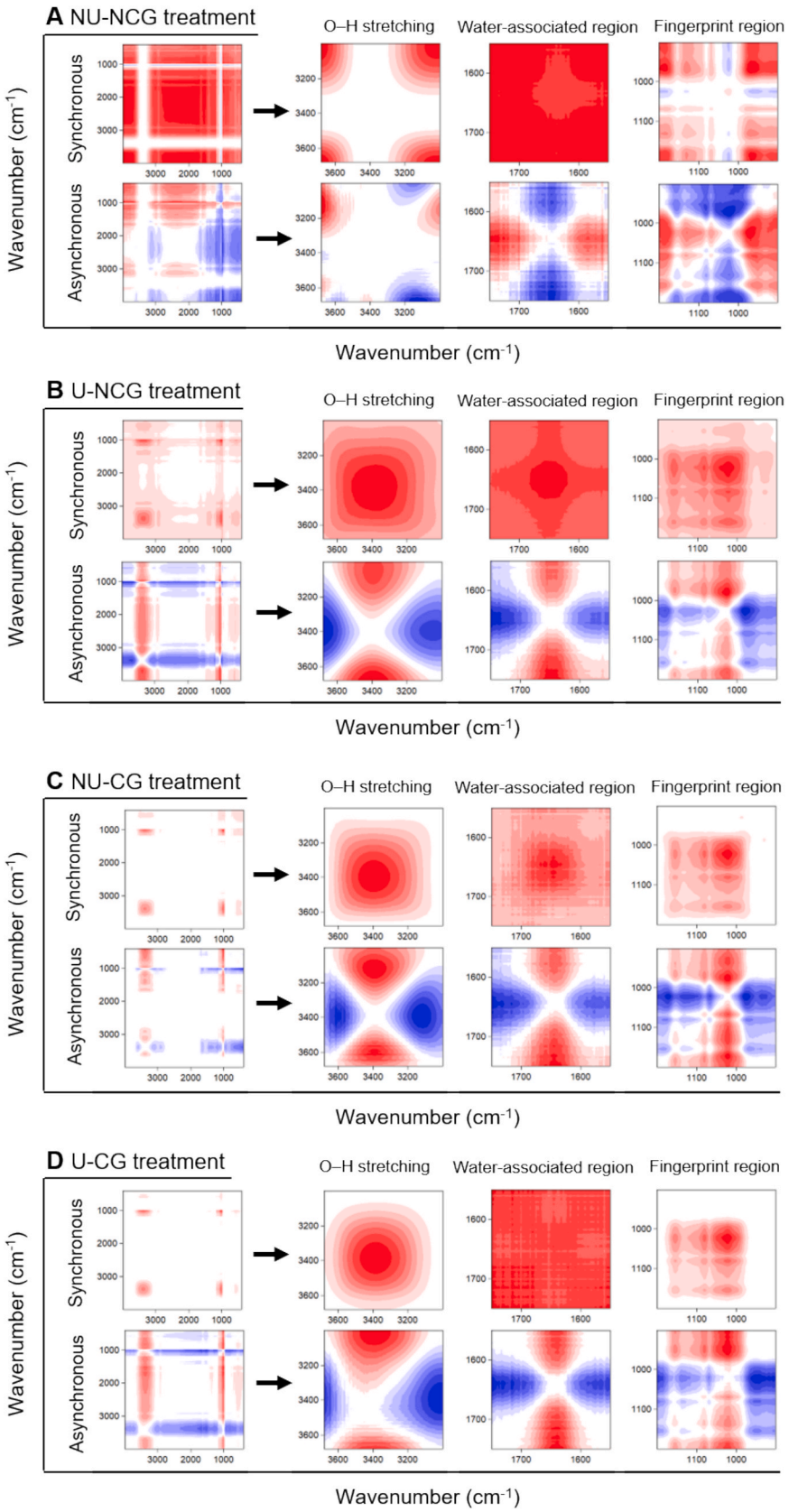


Fig. 10. Temperature-dependent two-dimensional correlation spectra of corn starch under different treatment conditions. The four spectral series correspond to NU-NCG, U-NCG, NU-CG, and U-CG samples at intervention temperatures of 60, 69, and 73 °C. For each series, the upper and lower rows show the synchronous and asynchronous spectra, respectively. Enlarged maps are presented for the O–H stretching region (3680–3000 cm^{-1}), the water-associated region (1750–1550 cm^{-1}), and the starch fingerprint region (1200–900 cm^{-1}). Red and blue contours indicate positive and negative correlation intensities, respectively.

Table 5
DSC gelatinization parameters of corn starch after thermal and ultrasonic treatments.

Sample	T_o (℃)	T_p (℃)	T_c (℃)	T_c-T_o (℃)	ΔH (J/g)
Corn Starch	69.11 ± 0.11^{b}	73.00 ± 0.13^{b}	76.57 ± 0.30 ^{a}	7.47 ± 0.19 ^{a}	1.87 ± 0.03 ^{a}
60-NU-NCG	68.60 ± 0.14^{c}	72.12 ± 0.22^{c}	75.52 ± 0.20 ^{bc}	6.93 ± 0.08^{b}	1.38 ± 0.03^{c}
60-U-NCG	68.46 ± 0.03^{c}	71.95 ± 0.12^{c}	75.22 ± 0.09^{c}	6.76 ± 0.10^{b}	1.63 ± 0.01^{b}
69-NU-NCG	72.29 ± 0.21 ^{a}	73.99 ± 0.30 ^{a}	75.93 ± 0.20^{b}	3.64 ± 0.06^{c}	0.15 ± 0.04 ^{d}

Values are expressed as the mean ± standard deviation (n = 3). Different lowercase letters within the same column indicate significant differences according to one-way ANOVA followed by Tukey's test ($p < 0.05$). Parameters are not reported for samples without a detectable endothermic transition peak.

gelatinization endothermic transition under the DSC conditions. Subsequently, heating to 95 ℃ further reduced the detectable gelatinization enthalpy in the CG samples [13]. Overall, the DSC results demonstrate that the thermal responses of starch samples varied depending on the ultrasound intervention condition during the gelatinization transition [64]. Ultrasound at 60 °C induced limited changes in detectable ordered structures, whereas ultrasound applied at 69 °C was associated with the disappearance of the detectable gelatinization transition [65]. For the 95 °C-treated samples, no detectable gelatinization endothermic transition was observed in DSC thermograms (Fig. 11), supporting their use as a fully processed reference condition under the applied treatment conditions.

The conceptual framework in Fig. 12 integrates the experimental observations with the hierarchical structural organization of starch. During the early transition region, hydration primarily occurs within more accessible amorphous regions, while a substantial proportion of ordered nanocrystalline domains remains detectable. As the intervention temperature approaches the gelatinization transition, increased hydration and molecular mobility are accompanied by progressive loss of detectable long-range crystalline order and changes in local molecular organization. Near the peak transition region, the marked attenuation of XRD diffraction features and DSC endothermic response indicate extensive loss of detectable long-range order. Accordingly, the nanocrystalline structures shown in Fig. 12 should be regarded as a conceptual representation based on current structural models of starch rather than as direct evidence of specific nanocrystal transformation in the present study.

4. Conclusion

This study demonstrates that the response of corn starch to thermo-ultrasonic treatment depends strongly on its structural state when ultrasound is applied during gelatinization.

(1) At 60 °C, ultrasound primarily enhanced starch hydration and swelling, while the principal orthorhombic diffraction features and the consistency and viscoelasticity of the final paste were largely preserved.
(2) At 69 and 73 °C, ultrasound produced greater granule disruption and a pronounced loss of detectable long-range crystalline order, accompanied by changes in local molecular organization and reduced consistency and viscoelastic strength after subsequent gelatinization.

Overall, gelatinization-stage-directed thermo-ultrasonic treatment provides a practical strategy for regulating starch structural evolution and final paste functionality by selecting the appropriate intervention stage. This study establishes a conceptual framework for tailoring starch functionality in thermal processing applications, providing a eco-friendly strategy for regulateing starch hydration-related properties and viscoelasticity for targeted end-use applications.

CRediT authorship contribution statement

Houhua Wang: Writing – review & editing, Writing – original draft, Visualization, Software, Methodology, Investigation, Data curation,

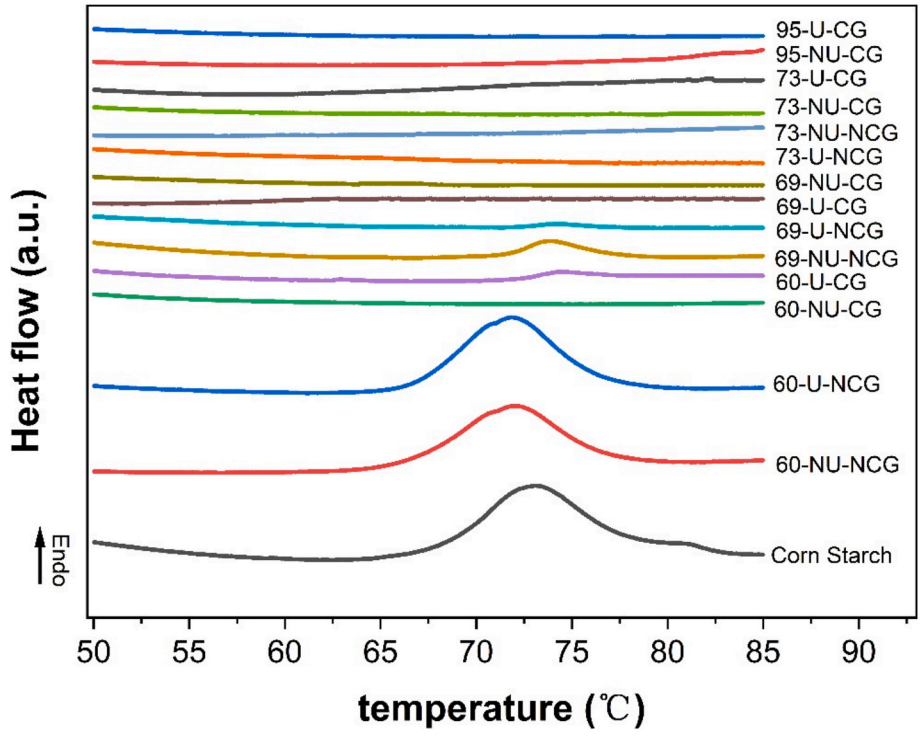


Fig. 11. DSC thermograms of native and treated corn starch.

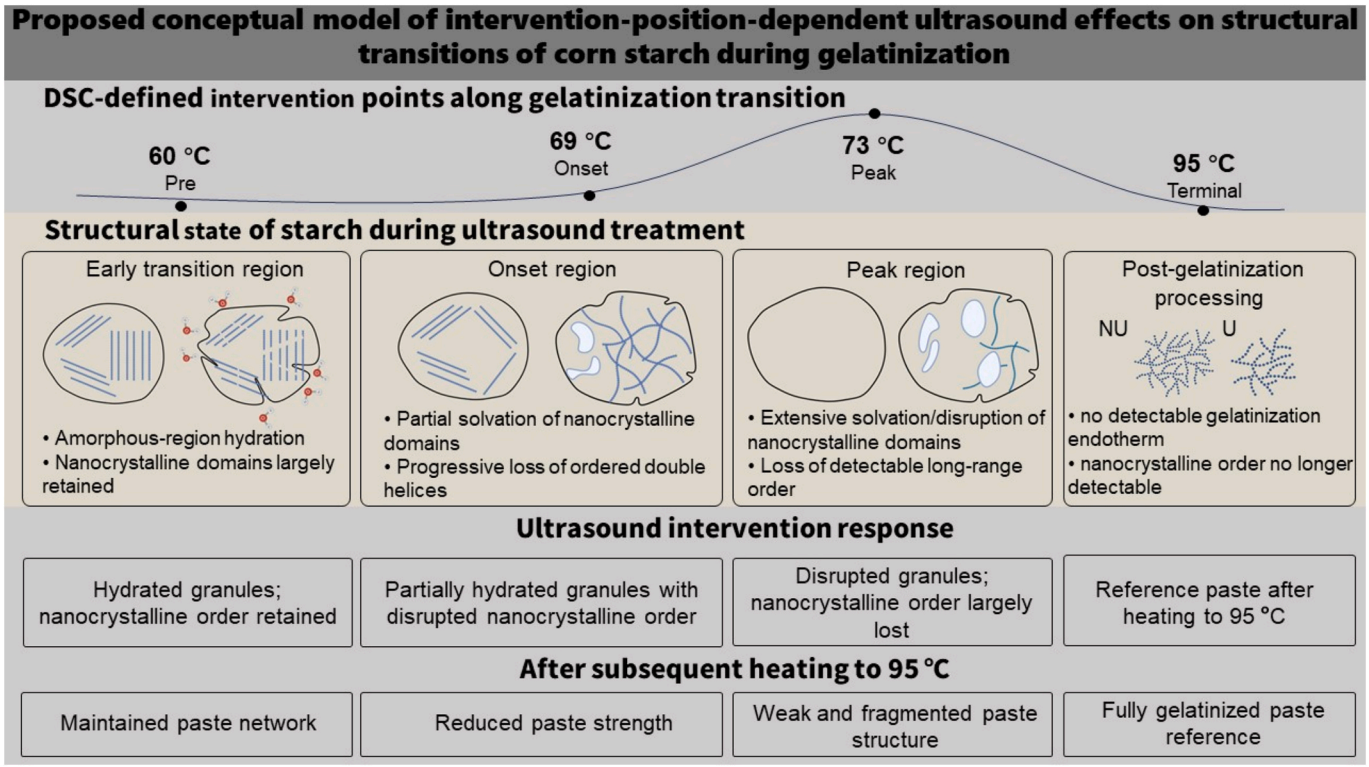


Fig. 12. Conceptual framework illustrating the intervention-position-dependent structural responses of corn starch to thermo-ultrasonic treatment during the gelatinization transition. The intervention temperatures of 60, 69, and 73 °C represent different positions along the DSC-derived gelatinization transition, while 95 °C serves as a fully processed reference condition. The schematic summarizes the immediate structural responses of samples collected after intervention (NCG) and the corresponding paste behavior after subsequent heating to 95 °C (CG), incorporating changes in granule hydration, structural disruption, and detectable nanocrystalline order.

Conceptualization. **Yuanyuan Li:** Software, Methodology, Investigation. **Tianpeng Chen:** Formal analysis, Conceptualization. **Wenjun Wang:** Writing – review & editing, Project administration. **Donghong Liu:** Supervision, Project administration. **Shuang Qiu:** Writing – review & editing, Validation, Project administration, Funding acquisition, Conceptualization.

Declaration of competing interest

The authors declare that they have no known competing financial interests or personal relationships that could have appeared to influence the work reported in this paper.

Acknowledgments

This study was financially supported by the Guangxi Key Research and Development Program (2025FN9607667), the Jiaxing Key Project for Industrial Development and Technological Innovation Research (2025AC038), and the Joint Fund of Zhejiang Provincial Natural Science Foundation of China (LJXSQY26C200001).

References

[1] M. Majzoobi, A. Farahnaky, Granular cold-water swelling starch; properties, preparation and applications, a review, Food Hydrocoll. 111 (2021), https://doi.org/10.1016/j.foodhyd.2020.106393.
[2] S. Hedayati, F. Shahidi, M. Majzoobi, A. Koocheki, A. Farahnaky, Structural, rheological, pasting and textural properties of granular cold water swelling maize starch: effect of NaCl and CaCl2, Carbohydr. Polym. 242 (2020), https://doi.org/10.1016/j.carbpol.2020.116406.
[3] P.E. Martinez-Munoz, E. Gutierrez-Cortez, M.I. Hernandez-Urbiola, A. Lopez-Leon, O.Y. Barron-Garcia, M.E. Rodriguez-Garcia, Physicochemical characterization of isolated nanocrystals in starch and isolated rice starch: A new perspective, Food Chem. 495 (2025), https://doi.org/10.1016/j.foodchem.2025.146590.
[4] Y. Takahashi, T. Kumano, S. Nishikawa, Crystal structure of B-amylose, Macromolecules 37 (18) (2004) 6827–6832, https://doi.org/10.1021/ma0490956.
[5] H. Ma, M. Liu, Y. Liang, X. Zheng, L. Sun, W. Dang, J. Li, L. Li, C. Liu, Research progress on properties of pre-gelatinized starch and its application in wheat flour products, Grain Oil Sci. Technol. 5 (2) (2022) 87–97, https://doi.org/10.1016/j.gaost.2022.01.001.
[6] K.K.T. Goh, O. Yuliarti, G.T.T. Yeo, C.C. Or, Effect of ultrasonication on low-acetylated gellan gum gel properties, Food Hydrocoll. 49 (2015) 240–247, https://doi.org/10.1016/j.foodhyd.2015.04.002.
[7] C.A. Maestri, M. Abrami, S. Hazan, E. Chistè, Y. Golan, J. Rohrer, A. Bernkop-Schnürch, M. Grassi, M. Scarpa, P. Bettotti, Role of sonication pre-treatment and cation valence in the sol-gel transition of nano-cellulose suspensions, Sci. Rep. 7 (2017), https://doi.org/10.1038/s41598-017-11649-4.
[8] F. Zendeboodi, A. Farahnaky, M.M. Gholian, Structural changes and stress relaxation behavior of κ-carrageenan cold-processed gels: effects of ultrasonication time and power, J. Texture Stud. 50 (6) (2019) 465–473, https://doi.org/10.1111/jtxs.12457.
[9] A. Imberty, H. Chanzy, S. Perez, A. Buleon, V. Tran, THE DOUBLE-HELICAL NATURE OF THE CRYSTALLINE PART OF A-STARCH, J. Mol. Biol. 201 (2) (1988) 365–378, https://doi.org/10.1016/0022-2836(88)90144-1.
[10] F. Zhu, Impact of ultrasound on structure, physicochemical properties, modifications, and applications of starch, Trends Food Sci. Technol. 43 (1) (2015) 1–17, https://doi.org/10.1016/j.tifs.2014.12.008.
[11] M.E. Rodriguez-Garcia, M.A. Hernandez-Landaverde, J.M. Delgado, C.F. Ramirez-Gutierrez, M. Ramirez-Cardona, B.M. Millan-Malo, S.M. Londoño-Restrepo, Crystalline structures of the main components of starch, Curr. Opin. Food Sci. 37 (2021) 107–111, https://doi.org/10.1016/j.cofs.2020.10.002.
[12] M. Sujka, Ultrasonic modification of starch - impact on granules porosity, Ultrason. Sonochem. 37 (2017) 424–429, https://doi.org/10.1016/j.ultsonch.2017.02.001.
[13] G. Li, X.H. Ge, C.S. Guo, B.G. Liu, Effect of ultrasonic treatment on structure and physicochemical properties of pea starch, Foods 12 (13) (2023), https://doi.org/10.3390/foods12132620.
[14] A. Golkar, J.M. Milani, A. Motamedzadegan, R.E. Kenari, Modification of corn starch by thermal-ultrasound treatment in presence of Arabic gum, Sci. Rep. 12 (1) (2022), https://doi.org/10.1038/s41598-022-23836-z.
[15] Y. Iida, T. Tuziuti, K. Yasui, A. Towata, T. Kozuka, Control of viscosity in starch and polysaccharide solutions with ultrasound after gelatinization, Innov. Food Sci. Emerg. Technol. 9 (2) (2008) 140–146, https://doi.org/10.1016/j.ifset.2007.03.029.
[16] L.Y. Rong, W.Q. Fei, Z.J. Wang, X.X. Chen, H.L. Wen, J.H. Xie, M.Y. Shen, Modulation of starch digestibility using non-thermal processing techniques: A

review, Grain Oil Sci. Technol. 7 (3) (2024) 209–218, https://doi.org/10.1016/j.gaost.2024.05.002.
[17] N. Singh, J. Singh, L. Kaur, N.S. Sodhi, B.S. Gill, Morphological, thermal and rheological properties of starches from different botanical sources, Food Chem. 81 (2) (2003) 219–231, https://doi.org/10.1016/s0308-8146(02)00416-8.
[18] S. Nara, T. Komiya, Studies on the relationship between water1044 satured state and crystallinity by the diffraction 1045 method for moistened potato starch, Starch/Stärke 35 (12) (1983) 407–410, https://doi.org/10.1002/star.19830351202.
[19] S. Morita, Y. Ozaki,I. Noda, Global phase angle description of generalized two-dimensional correlation spectroscopy: 2. Its application to temperature-dependent infrared spectra of a Langmuir-Blodgett film of 2-dodecyl-7,7,8,8-tetracyanoquinodimethane, Appl. Spectrosc. 55(12) (2001) 1622-1627 https://doi.org/10.1366/0003702011954198.
[20] S. Morita, Y. Ozaki,I. Noda, Global phase angle description of generalized two-dimensional correlation spectroscopy: 1. Theory and its simulation for practical use, Appl. Spectrosc. 55(12) (2001) 1618-1621 https://doi.org/10.1366/0003702011954189.
[21] S.T. Sun, H. Tang, P.Y. Wu, X.H. Wan, Supramolecular self-assembly nature of a novel thermotropic liquid crystalline polymer containing no conventional mesogens, Phys. Chem. Chem. Phys. 11 (42) (2009) 9861–9870, https://doi.org/10.1039/b909914j.
[22] A.J. Vela, M. Villanueva, F. Ronda, Ultrasonication: an efficient alternative for the physical modification of starches, Flours and Grains, Foods 13 (15) (2024), https://doi.org/10.3390/foods13152325.
[23] H.V. Nguyen, P.X. Huynh, T.C. Kha, Ultrasound-induced modification of durian starch (durio zibethinus) for gel-based applicationsphysicochemical and thermal properties, Gels 11 (4) (2025), https://doi.org/10.3390/gels11040296.
[24] C.D. Chi, X.X. Li, Y.P. Zhang, S. Miao, L. Chen, L. Li, Y. Liang, Understanding the effect of freeze-drying on microstructures of starch hydrogels, Food Hydrocoll. 101 (2020), https://doi.org/10.1016/j.foodhyd.2019.105509.
[25] Y.Y. Zhao, S.M. Qiao, X.H. Zhu, J.N. Guo, G.Q. Peng, X.X. Zhu, R.L. Gu, Z.Y. Meng, Z.A. Wu, H. Gan, D. Guifang, Y.G. Jin, S.C. Liu, Y.B. Sun, Effect of different drying methods on the structure and properties of porous starch, Heliyon 10 (10) (2024), https://doi.org/10.1016/j.heliyon.2024.e31143.
[26] R. Torres-Gallo, R. Andrade-Pizarro, D.F. Tirado, A. Chávez-Salazar, F. J. Castellanos-Galeano, Mechanochemical effects of high-intensity ultrasound on dual starch modification of mango cotyledons, Agriengineering 7 (6) (2025), https://doi.org/10.3390/agriengineering7060190.
[27] M. Jafari, A. Koocheki, Impact of ultrasound treatment on the physicochemical and rheological properties of acid hydrolyzed sorghum starch, Int. J. Biol. Macromol. 256 (2024), https://doi.org/10.1016/j.ijbiomac.2023.128521.
[28] L.P. Martínez-Padilla, Rheology of liquid foods under shear flow conditions: Recently used models, J. Texture Stud. 55 (1) (2024), https://doi.org/10.1111/jtxs.12802.
[29] A. Golkar, J.M. Milani, A. Motamedzadeghan, R.E. Kenari, Physicochemical, structural, and rheological characteristics of corn starch after thermal-ultrasound processing, Food Sci. Technol. Int. 29 (2) (2023) 168–180, https://doi.org/10.1177/10820132211069242.
[30] N. Kang, Y.J. Zuo, L. Hilliou, M. Ashokkumar, Y. Hemar, Viscosity and hydrodynamic radius relationship of high-power ultrasound depolymerised starch pastes with different amylose content, Food Hydrocoll. 52 (2016) 183–191, https://doi.org/10.1016/j.foodhyd.2015.06.017.
[31] H. Nie, C. Li, P.H. Liu, C.Y. Lei, J.B. Li, Retrogradation, gel texture properties, intrinsic viscosity and degradation mechanism of potato starch paste under ultrasonic irradiation, Food Hydrocoll. 95 (2019) 590–600, https://doi.org/10.1016/j.foodhyd.2017.08.035.
[32] A.M. Amini, S.M.A. Razavi, S.A. Mortazavi, Morphological, physicochemical, and viscoelastic properties of sonicated corn starch, Carbohydr. Polym. 122 (2015) 282–292, https://doi.org/10.1016/j.carbpol.2015.01.020.
[33] E.J.C. Parra, P. Palavecino, P.D. Ribotta, M.C. Penci, Effect of ultrasound treatment on structural and physical properties of native maize starch, Plant Foods Hum. Nutr. 80 (1) (2025), https://doi.org/10.1007/s11130-024-01285-5.
[34] A. Yilmaz, N. Tugrul, Effect of ultrasound-microwave and microwave-ultrasound treatment on physicochemical properties of corn starch, Ultrason. Sonochem. 98 (2023), https://doi.org/10.1016/j.ultsonch.2023.106516.
[35] S. Pesek, R. Silaghi-Dumitrescu, The Iodine/iodide/starch supramolecular complex, Molecules 29 (3) (2024), https://doi.org/10.3390/molecules29030641.
[36] E. Abedi, M. Sayadi, A. Karimzadeh, M. Sourghali, P. Zhang, Micro N2-bubble-assisted esterification or crosslinking of corn starch by citric, lactic and malic acid: facilitating the reaction medium under hydrodynamic cavitation, Int. J. Biol. Macromol. 303 (2025), https://doi.org/10.1016/j.ijbiomac.2025.140714.
[37] E. Abedi, H.H. Gahruie, S.M.H. Hosseini, P. Zhang, Impact of hydrodynamic cavitation-assisted microbubble with N2, CO2, and air on pasting, morphological, and thermal properties of starches from different botanical origins, Int. J. Biol. Macromol. 301 (2025), https://doi.org/10.1016/j.ijbiomac.2025.140253.
[38] J.N. Yang, F.W. Xie, W.Q. Wen, L. Chen, X.Q. Shang, P. Liu, Understanding the structural features of high-amylose maize starch through hydrothermal treatment, Int. J. Biol. Macromol. 84 (2016) 268–274, https://doi.org/10.1016/j.ijbiomac.2015.12.033.
[39] Q. Xu, S.Y. Sang, Y.L. Wang, C.P. Tan, L. Peplowski, X.J. Tang, M. Meng, H.T. Lei, Effect of glycerol monostearate on the structure and retrogradation of gelatinized wheat starch at high temperature, Grain Oil Sci. Technol. 8 (3) (2025) 175–181, https://doi.org/10.1016/j.gaost.2025.05.003.
[40] K.T. Han, H.R. Kim, T.W. Moon, S.J. Choi, Isothermal and temperature-cycling retrogradation of high-amylose corn starch: impact of sonication on its structural and retrogradation properties, Ultrason. Sonochem. 76 (2021), https://doi.org/10.1016/j.ultsonch.2021.105650.
[41] E. Abedi, M. Sayadi, K. Pourmohammadi, Effect of freezing-thawing pre-treatment on enzymatic modification of corn and potato starch treated with activated a-amylase: investigation of functional properties, Food Hydrocoll. 129 (2022), https://doi.org/10.1016/j.foodhyd.2022.107676.
[42] I. Tan, B.M. Flanagan, P.J. Halley, A.K. Whittaker, M.J. Gidley, A method for estimating the nature and relative proportions of amorphous, single, and double-helical components in starch granules by 13C CP/MAS NMR, Biomacromolecules 8 (3) (2007) 885–891, https://doi.org/10.1021/bm060988a.
[43] B.M. Flanagan, M.J. Gidley, F.J. Warren, Rapid quantification of starch molecular order through multivariate modelling of 13C CP/MAS NMR spectra, Chem. Commun. 51 (80) (2015) 14856–14858, https://doi.org/10.1039/c5cc06144j.
[44] S. Wu, J.L. Yu, L. Copeland, S.J. Wang, Novel method for characterizing short-range molecular order in noncrystalline starch by 13C CP/MAS NMR, J. Agric. Food Chem. 74 (3) (2026) 3146–3156, https://doi.org/10.1021/acs.jafc.5c10437.
[45] A. Nowacka-Perrin, T. Steglich, D. Topgaard, D. Bernin, In situ 13C solid-state polarization transfer NMR to follow starch transformations in food, Magn. Reson. Chem. 60 (7) (2022) 671–677, https://doi.org/10.1002/mrc.5253.
[46] J. Moreno-Zaragoza, J. Alvarez-Ramirez, S. Dhital, L.A. Bello-Pérez, Chromatographic analysis of branched and debranched starch structure: variability of their results, Int. J. Biol. Macromol. 281 (2024), https://doi.org/10.1016/j.ijbiomac.2024.136639.
[47] Y.J. Chang, X.X. Yan, Q. Wang, L.L. Ren, J. Tong, J. Zhou, High efficiency and low cost preparation of size controlled starch nanoparticles through ultrasonic treatment and precipitation, Food Chem. 227 (2017) 369–375, https://doi.org/10.1016/j.foodchem.2017.01.111.
[48] L.H. Han, J.P. Huang, Y.T. Yu, K. Thakur, Z.J. Wei, L.Y. Xiao, X.F. Yang, The alterations in granule, shell, blocklets, and molecular structure of pea starch induced by ultrasound, Int. J. Biol. Macromol. 240 (2023) 1–9, https://doi.org/10.1016/j.ijbiomac.2023.124319.
[49] Z.G. Luo, X. Fu, X.W. He, F.X. Luo, Q.Y. Gao, S.J. Yu, Effect of ultrasonic treatment on the physicochemical properties of maize starches differing in amylose content, Starch/Stärke 60 (11) (2008) 646–653, https://doi.org/10.1002/star.200800014.
[50] R.A. Cave, S.A. Seabrook, M.J. Gidley, R.G. Gilbert, Characterization of starch by size-exclusion chromatography: the limitations imposed by shear scission, Biomacromolecules 10 (8) (2009) 2245–2253, https://doi.org/10.1021/bm900426n.
[51] A. Szwengiel, P. Kubiak, Molecular dispersion of starch as a crucial parameter during size-exclusion chromatography, Foods 9 (9) (2020), https://doi.org/10.3390/foods9091204.
[52] F. Zhong, W. Yokoyama, Q. Wang, C.F. Shoemaker, Rice starch, amylopectin, and amylose: molecular weight and solubility in dimethyl sulfoxide-based solvents, J. Agric. Food Chem. 54 (6) (2006) 2320–2326, https://doi.org/10.1021/jf051918i.
[53] J. Zhang, M. Zhang, X. Bai, Y. Zhang, C. Wang, The impact of high hydrostatic pressure treatment time on the structure, gelatinization and thermal properties and in vitro digestibility of oat starch, Grain Oil Sci. Technol. 5 (1) (2022) 1–12, https://doi.org/10.1016/j.gaost.2022.01.002.
[54] R. Roohi, E. Abedi, S.M.B. Hashemi, Ultrasound-assisted starch hydrolyzing by alpha-amylase: Implementation of computational fluid dynamics, acoustic field determination, and rheology modeling, Ultrason. Sonochem. 103 (2024), https://doi.org/10.1016/j.ultsonch.2024.106785.
[55] B.G. Xu, A.Q. Ren, J.N. Chen, H.Y. Li, B.X. Wei, J. Wang, S.M.R. Azam, B. Bhandari, C.S. Zhou, H.L. Ma, Effect of multi-mode dual-frequency ultrasound irradiation on the degradation of waxy corn starch in a gelatinized state, Food Hydrocoll. 113 (2021), https://doi.org/10.1016/j.foodhyd.2020.106440.
[56] R.N. Tiozon Jr., A.P. Bonto, J.A.H. Padua, E.G.A. Elbo, J.R. Sampang, K. Kamkajon, D.H. Camacho, K. Thumanu, Investigating the effect of ultrasonication on the molecular structure of potato starch using synchrotron-based infrared spectroscopy, Biointerface Res. Appl. Chem. 12 (5) (2022) 6686–6698. https://doi.org/10.33263/briac123.66866698.
[57] H.J. An, Q.Y. Ma, F. Zhang, C. Zhai, J.F. Sun, Y.W. Tang, W.X. Wang, Insight into microstructure evolution during starch retrogradation by infrared and Raman spectroscopy combined with two-dimensional correlation spectroscopy analysis, Food Hydrocoll. 146 (2024), https://doi.org/10.1016/j.foodhyd.2023.109174.
[58] I. Noda, GENERALIZED 2-DIMENSIONAL CORRELATION METHOD APPLICABLE TO INFRARED, RAMAN, AND OTHER TYPES OF SPECTROSCOPY, Appl. Spectrosc. 47 (9) (1993) 1329–1336, https://doi.org/10.1366/0003702934067694.
[59] H. Shinzawa, J. Mizukado, Hydrogen/deuterium (H/D) exchange of gelatinized starch studied by two-dimensional (2D) near-infrared (NIR) correlation spectroscopy, Spectrochim. Acta A Mol. Biomol. Spectrosc. 197 (2018) 138–141, https://doi.org/10.1016/j.saa.2017.12.065.
[60] F.J. Warren, M.J. Gidley, B.M. Flanagan, Infrared spectroscopy as a tool to characterise starch ordered structure-a joint FTIR-ATR, NMR, XRD and DSC study, Carbohydr. Polym. 139 (2016) 35–42, https://doi.org/10.1016/j.carbpol.2015.11.066.
[61] I. Chakraborty, N. Pooja, S.S. Mal, U.C. Paul, M.H. Rahman, N. Mazumder, An insight into the gelatinization properties influencing the modified starches used in food industry: A review, Food Bioprocess Technol. 15 (6) (2022) 1195–1223, https://doi.org/10.1007/s11947-022-02761-z.
[62] Y.X. Zuo, F.L. Zou, M. Yang, G.F. Xu, J.H. Wu, L.J. Wang, H.Y. Wang, Effects of plasma-activated water combined with ultrasonic treatment of corn starch on structural, thermal, physicochemical, functional, and pasting properties, Ultrason. Sonochem. 108 (2024), https://doi.org/10.1016/j.ultsonch.2024.106963.

[63] M.M. Jiang, K. Zhang, W.X. Zhu, W.F. Wu, X.J. Wang, Y.Q. Cheng, C.Y. Che, Y. G. Liu, The effect of ultrasonic treatment on the physicochemical and pasting properties of pre-gelatinized Coix seed starch, Ultrason. Sonochem. 125 (2026), https://doi.org/10.1016/j.ultsonch.2026.107742.
[64] R. Roohi, E. Abedi, S.M.B. Hashemi, M. Akbari, Effect of ultrasound geometry on the production efficiency of damaged starch: determining rheology parameters, and non-isothermal reaction kinetics, Ultrason. Sonochem. 106 (2024), https://doi.org/10.1016/j.ultsonch.2024.106882.
[65] B. Teng, C. Zhang, H. Wang, Impact of partial gelatinization on structure, physicochemical and enzymatic digestion properties of rice starch used for rice noodle-making, Polymers 17 (22) (2025), https://doi.org/10.3390/polym17223003.